RESEARCH ARTICLE

Spatial and temporal variations of geochemical processes and toxicity of water, sediments, and suspended solids in Sibuti River Estuary, NW Borneo

Rakesh Roshan Gantayat[1,2] · Prasanna Mohan Viswanathan[1] · Nagarajan Ramasamy[1] · Chidambaram Sabarathinam[3]

Abstract

A comprehensive geochemical study was conducted in the Sibuti River estuary by considering water, suspended solids (SS), and sediment samples from 36 stations during southwest monsoon (SWM) and northeast monsoon (NEM). In this study, the distribution of in situ parameters, major ions, nutrients, trace metals, and isotopes (δD, $\delta^{18}O$) were analyzed in water samples, whereas sediments and SS were studied for trace metals. The distribution revealed that suspended solids were the major carrier of Cd, Zn, and Mn, whereas sediments worked as a major source of Co, Cr, Ba, Se, Cu, and Pb. Na-Cl water type and ion exchange dominated the lower part of the estuary during both seasons. However, the mixed mechanism of Ca–Cl, Ca–Mg–Cl, and higher weathering indicated reverse ion exchange in the intermediate and upper parts of the estuary. Isotopic signatures of δD and $\delta^{18}O$ in estuarine water indicate that the precipitation over the Limbang area dominates during SWM, whereas higher evaporation was confirmed during NEM. The factor analysis revealed that seawater influence in the estuary majority controlled the water chemistry irrespective of seasons. Major ions were mainly regulated by the tidal influence during the low flow time of the river (SWM), whereas the mixing mechanism of weathering and seawater controlled the concentrations during NEM. Nutrients such as NO_3, SO_4^{2-}, NH_3, and NH_4^+ mainly originated from the agricultural fields and nitrification along with ammonification were responsible for the recycling of such nutrients. Trace metals except Cd were found to be geogenic in nature and originating mainly from the oxidation of pyrites present in the sandstone and mudstones of the Sibuti Formation. Redox condition was catalyzed by microorganisms near the river mouth, whereas Al-oxyhydroxides and Fe-oxyhydroxides complexes in the intermediate and upper part under oxygenated conditions controlled the absorption of metals. Overall, the estuary was found to be absorptive in nature due to ideal pH conditions and was confirmed by the saturation index (SI) of minerals.

Keywords Geochemistry · Ion exchange · Redox · Absorption · Metal mobility · Sibuti River · Estuary

✉ Prasanna Mohan Viswanathan
  prasanna@curtin.edu.my

1 Department of Applied Sciences, Faculty of Engineering and Science, Curtin University Malaysia, CDT 250, 98009 Miri, Sarawak, Malaysia

2 Department of Hydrology, University of Zululand, Kwadlangezwa, South Africa

3 Water Research Center, Kuwait Institute for Scientific Research, Safat, Kuwait

Introduction

Globally, rivers are the essential participants of geochemical, biochemical, and elemental cycles due to their nature of being a primary facilitator in the transport of terrestrial inputs through sediments, suspended and in dissolved form (Reiman et al. 2018). The key drivers of such changes in a river's ecosystem are always the inputs by the headwaters, in its catchment area or floodplains. On the other hand, estuaries are the transitional zone of the river where the mixing of two water masses (seawater and river water) of distinct physico-chemical properties takes place while working as a geochemical filter for contaminants carried in form of sediment (suspended and bed load) and dissolved load (Guinoiseau et al. 2016; Koukina et al. 2021). The origin of these

contaminants generally attributes to anthropogenic sources such as agriculture and urbanized run-off (Somura et al. 2012; Priya et al. 2014; Frazar et al. 2019; Asha et al. 2020; Huang et al. 2020) and natural sources such as weathering of rocks in the basinal region (Pavoni et al. 2021), which contributes the majority of the solutes and solid matters to the river system (Martin and Whitfield 1983; Lintern et al. 2018).

The primary functions of the river is mainly controlled by the three interfaces such as water, suspended particles, and sediment load. Sediments are considered as the most important interface to be paid attention to as the global contribution of river-derived sediments comprises up to 95% of the material entering the world's oceans (Lučić et al. 2019). In addition to that, 30 to 98% of toxic materials like metals from geogenic/anthropogenic sources transported by rivers get deposited on sediments under varying environmental conditions (Gibbs 1973; Yang and Wang 2017). The study of sediment composition in estuaries helps to reflect the geochemical nature of the river basin and helps to elucidate the overall character of the material transported by rivers from adjacent land areas, derived from shoreline erosion, carried by marine currents from external sources, and produced in situ by organisms and contribution by human activities (Prabakaran et al. 2020). On the other hand, rivers around the world carry 13.5×10^9 tons of suspended solids towards the sea (Eisma 1988), and estuaries work as geochemical and biochemical reactors that modify the river fluxes and composition of terrestrial inputs within its influencing territory (Sholkovitz and Szymczak 2000; Koukina et al. 2021). Such processes are mainly controlled by physical and chemical factors such as hydrodynamic mixing due to volatile tidal gradient (Salas-Monreal and Valle-Levinson 2008; Mathew and Winterwerp 2020) whereas fluvial effect and geomorphological processes coupled with rock-water interaction contribute the majority of weathered inputs and are highly dependent on seasonal rainfall (Ralston et al. 2013; Brantley et al. 2017; Mathew & Winterwerp 2020). In such an environment, cohesive aggregates play a major role in the sorption of various suspended and dissolved chemical constituents (Mehta 1989; Kronvang et al. 2003). The deviating nature of these particles from bedload sediments allows them to mobilize frequently and follow much shorter cycles than the resistant sediment particles at the bottom (Eisma 1988). The availability in the water table besides working as a medium between metals that are dissolved and in the solid phase, a much larger surface area, and the presence of clay minerals and organic matter which are far more surface-active than comparatively larger sediments allow them to absorb/desorb higher concentration of metals (Regnier and Wollast 1993).

Furthermore, the formation of turbidity maxima zones (TMZ) with enhanced sediment tapping zones (Ishak et al.

2001; Mathew and Winterwerp 2020) and complex chemical reactions such as dissolution/precipitation (Juen et al. 2015; Naderi et al. 2016; Vinh and Ouillon 2021), ion exchange (Patra et al. 2012; Cochran 2014; Hao et al. 2020), water density stratification leading oxidation–reduction process (e.g., Ishak et al. 2001; Walker et al. 2021; Tian 2020), flocculation (e.g., Karbassi et al. 2016; Zhang et al. 2020), and absorption/desorption (e.g., Hirst et al. 2017; Mohamed and Yaacob 2019; Zhou et al. 2020) are the major mechanisms behind metal transition between particulate and dissolved medium. In a similar manner, the tidal influence and seasonal rainfall also control the residence time of water in estuaries giving rise to nutrient cycles such as N-cycle and P-cycle (e.g., Zhu et al. 2018; Geisler et al. 2020; Wei et al. 2022) along with higher dissolution/precipitation of minerals in the estuarine system depending upon the CO_2 balance with atmosphere (Prasanna et al. 2010; Chidambaram et al. 2011; Naderi et al. 2016). The highly dynamic nature of estuaries with volatile tidal and geomorphological gradients provide a unique environment for such complex trace metal and nutrient cycling (Turner 1996).

The distribution of trace metals and nutrients in solid, liquid, and colloidal or particulate phases plays a major role in determining the water quality and health of estuarine and coastal ecosystems (Tomczak et al. 2019; Iglesias et al. 2020; Koukina et al. 2021). As a result, these inputs work as a foundation for the survival of aquatic life while assisting in the primary production of nutrients such as N and P and the structural development of organisms; they also can aggravate adverse impacts on coastal and estuarine biota along with human health when present in overwhelming quantity (Jezierska et al. 2009; Tchounwou et al. 2012; Reiman et al. 2018). In the case of tropical river basins, intense rainfall coupled with warm and humid climate leads to intense weathering and transportation of terrestrial materials towards coastal regions in a shorter period compared to temperate climates (Koukina et al. 2021). Therefore, the study of estuaries of such rivers are ideal to study the geochemistry of water, sediment, and suspended solids (SS).

One of such estuaries is the Sibuti River estuary in Sarawak, Borneo, which discharges directly into the South China Sea (SCS). The previous studies conducted in the river estuary have been very limited to nutrients and some physico-chemical parameters (Gandaseca et al. 2011; Saifullah et al. 2014). The quantification and distribution of major ions, nutrients, and trace metals in water, sediments, and suspended solids and their governing geochemical processes have been lacking and remain a major gap. Consequently, this study is aimed at (1) filling the gap with the help of a geochemical baseline study of water, sediment, and suspended solid phase and (2) gaining an understanding of chemical processes controlling these ions, nutrients, and trace metals in these three different phases. To achieve the

objectives of this study, a multivariate approach has been implemented, which includes (1) implementation of geochemical plots (e.g., Piper and Gibbs plots) for water and statistical techniques such as factor analysis and principal component analysis (PCA) for water, sediments, and suspended solids to study geochemistry; (2) thermodynamic stability between the solid and dissolved phase was analyzed using saturation index (SI) for water, whereas partition coefficient (K_d) coupled with Pearson's correlation was utilized to understand the metal transition between both phases, and (3) stable isotopes such as δD and $\delta^{18}O$ were integrated with the study to identify the source of precipitation and origin of water in the estuary.

Study area

The Sibuti River estuary is situated in the Miri zone in the north-western part of Sarawak, which is one of the states of Malaysia that covers part of Borneo Island. The river has a catchment area of 1020 km^2 (Tenaga 2003) and discharges into South China Sea. The river catchment receives an average seasonal rainfall similar to the regional rainfall (3126 to 3246 mm, average: 3022 mm) and spanning over 220 days a year. The rainfall in the study area follows a similar pattern as regional and is mainly regulated by PDO (Pacific Decadal Oscillation) as mentioned before bringing two monsoon seasons in a year such as southwest monsoon (SWM) and northeast monsoon (NEM). This monsoonal effect is mainly responsible for the hydrological balance in this region and for controlling the river run-offs (Krawczyk et al. 2020; Naciri et al. 2023; Browne et al. 2019). Similarly, the NE monsoon is associated with higher rainfall than the SW monsoon. The river receives tides at a maximum height of 2–3 m and falls under tide-dominated estuary, especially in micro-tidal type (tidal height: 2–3 m) (Boothroyd 1978), where limited tidal influence can be expected irrespective of the season. The estuary has more than 30 km of pristine mangrove and Nipa palm (Mangrove palm) forest in the vicinity with several agricultural fields, small towns such as Bekenu, and several villages that are present around the river. The major land use activity in the river basin is agriculture and is mainly concentrated around Bekenu and several other villages. Bekenu's growing agro-activity drives in this region are a major source of income for the locals. The main agricultural products of these areas might include palm tree plantation, pandan coconut plantation, lemon grass, ginger, turmeric, shallots, chilies, and other herbs (MANRED, Sarawak 2020). The river is also accompanied by several tributaries such as Sungai Tiris and Sungai Kejapil along its path and mainly drains the sedimentary terrains and agricultural lands along the way. The current study focuses mainly on the estuarine region of the river starting from the river mouth to Balau village.

Lithology

The river basin is mostly influenced by three major and six minor formations, namely, the Sibuti Formation, Lambir Formation, and alluvium near the coast, whereas the minor formations may include Miri, Belait, Tukau, Nyalau, Setap shale, and Tangap formations). The basin is mainly represented by sedimentary rocks ranging from Oligocene to Pliocene. Sibuti and Lambir formations have a prominent presence in the river basin and cover 500.43 and 238.201 km^2 of area, respectively. Both the formations are formed by the recycling, transportation, and deposition of sediments from the collision zone of the Rajang group (Nagarajan et al. 2015, 2017a) caused by the event termed as Sarawak orogeny (Hutchison 1996; Hutchison 2005). The Sibuti Formation is reported to be dominated by calcareous mudstone/shale and sandstone (Nagarajan et al. 2017a) with prominent marl lenses, thin limestone beds, and high content of fossils in it (Peng et al. 2004; Nagarajan et al. 2015). The siliciclastic sediments of this formation are rich in light minerals such as quartz, mica, calcite, minor feldspar and zeolites, and clay minerals (i.e., illite, chlority, and kaolinite), along with heavy minerals such as zircon, rutile, pyrite, and ilmenite (Nagarajan et al. 2015, 2019). The Lambir Formation is mainly comprised of sandstones, sandy intercalations with shale and siltstones, mudstone, and limestone. Mineralogically, sandstones are comprised of quartz, illite/muscovite, along with a minor amount of plagioclase, whereas limestone consists of calcite, ankerite, quartz, chlorite, illite/muscovite, and a trace amount of aragonite (Nagarajan et al. 2017a). In addition, mudstones of this formation are dominated by quartz, illite/muscovite, amorphous phase, chlorite, plagioclase, and calcite (Nagarajan et al. 2017a, 2019). Apart from these major lithological details, the concretion of pyrites was reported to be present in Sibuti Formation (Azrul NIsyam et al. 2013; Nagarajan et al. 2019) and Tukau Formation (Nagarajan et al. 2017b, 2022), and these formations are also part of the Sibuti River basin.

Materials and methods

Sample collection and preparation

To assess monsoonal inputs, their associated parameters, and changes in the estuarine system, the sampling processes were planned and executed during SWM and NEM periods. The tidal water in estuaries is the major short-term influencer of spatial and chemical changes due to the intrusion of saline water from the sea and is helpful in demarcating
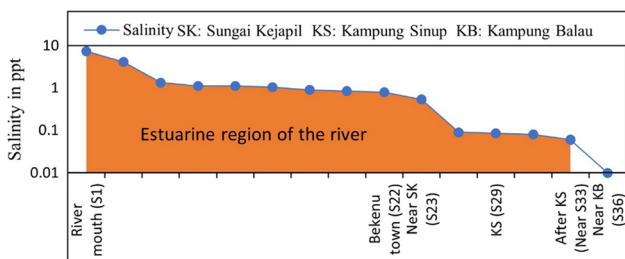
Fig. 1 Determined estuarine boundary during preliminary studies

during NEM. Sampling sites were selected depending upon some important aspects, such as the influence of tributaries, evidence of anthropogenic activities such as settlements and agricultural channels and meanders/major turnings. Thirty-six sites were confirmed, and 3 L of water samples were collected from each station in 3 clean polyethylene sample containers with depth reaching a maximum of 1–2 m at every station (Fig. 2). All 3 L of water were filtered with 0.45-μm Whatman filter paper, and total suspended solid (TSS) amount collected per liter of water through filtration was recorded for each station. The first bottle of water was used
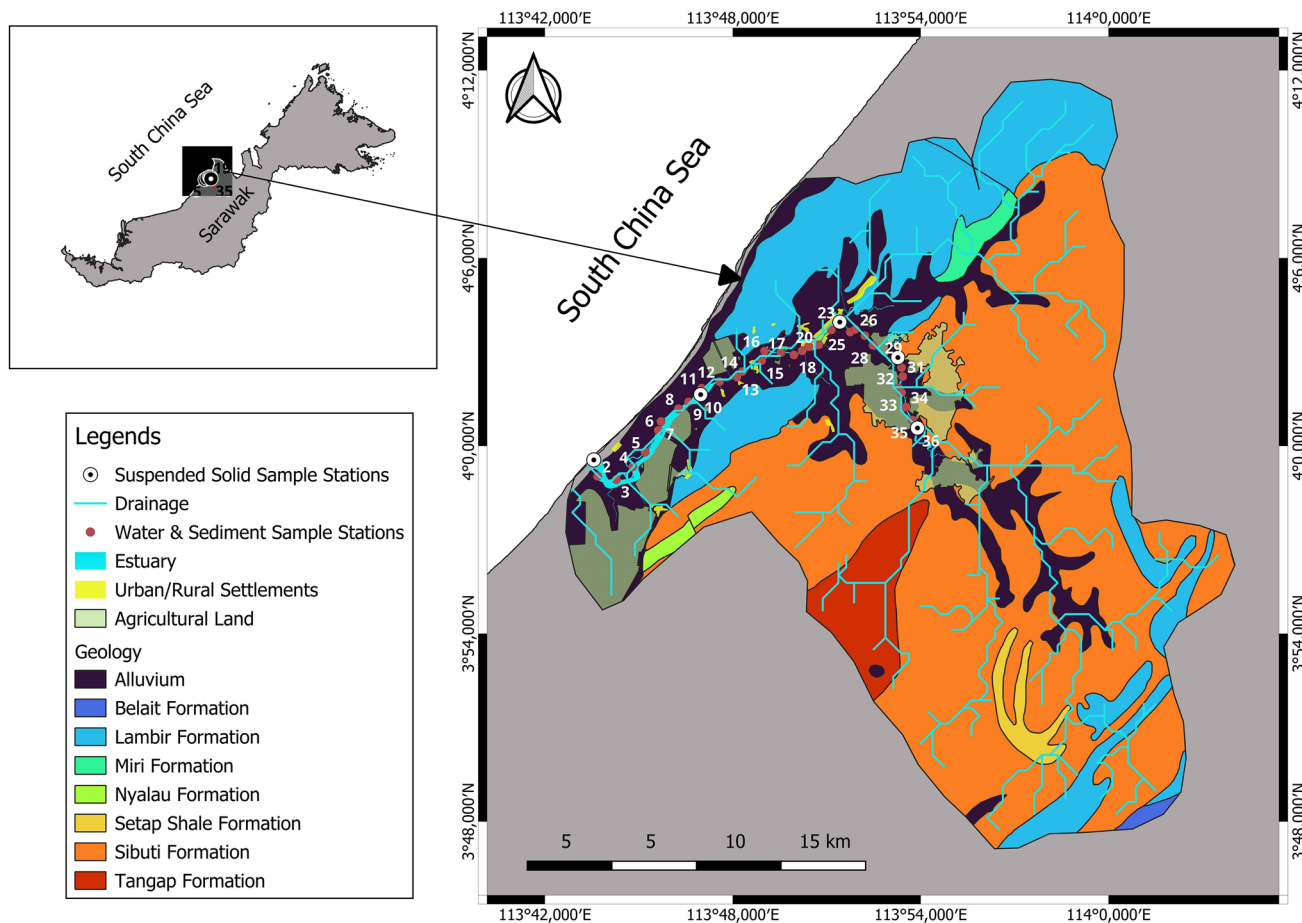

Fig. 2 Map of Sibuti river basin showing sampling stations, geological formations and land use pattern

the boundary of estuaries. Thus, high tidal conditions and salinity were taken into consideration during the demarcation of the estuarine boundary (Fig. 1). During the sampling process, observed tidal conditions were noted to assess their influence on riverine constituents during both seasons.

Water, bed load sediment, and suspended solid samples were collected in August 2017 (SW monsoon) and February 2018 (NE monsoon). High and low tidal conditions were observed during SWM on consecutive days whereas high-to-low tidal transition was observed on consecutive days

for nutrient (SO_4^{2-}, PO_4^{3-}, NH_3, NH_4^+, NO_3^-, and NO_3-N) analysis. The second bottle of water was used for the measurement of various major ion concentrations in water such as Cl^-, CO_3^-, HCO_3^-, Ca^{2+}, and Mg^{2+}, whereas the third bottle of water was acidified to pH < 2 for the determination of trace metals and major ions such as Na^+ and K^+ concentration in water using nitric acid (30%). These samples were stored in a refrigerator at 4 °C until further processes such as digestion and trace metal analysis. Similarly, 1 kg

of bed load sediments was collected from the same 36 stations using an Ekman grab sampler and stored in a plastic container and sealed to avoid any contamination. The central portion of the grab samples was considered to avoid contamination from the wall of the sampler. The sampler was washed on the river water before and after the sampling at each location and followed throughout the sampling. The sediment samples were collected in the middle of the river at each station. In addition to 1 L water samples collected from each stations to quantify the total suspended solids (TSS), ~20 L of water samples were collected at an interval of at least 10 km (Fig. 2) to obtain enough suspended solids for the bulk geochemical analysis. The interval has been considered to identify the changes occurring in the suspended solids amount and its constituents with respect to the river, its tributaries, and influence of tides in relation to the resuspension of the sediments along the estuary and various geochemical processes.

Field measurements

Physico-chemical parameters such as pH, temperature, electrical conductivity (EC), total dissolved solids (TDS), salinity, turbidity, and dissolved oxygen (DO) were measured in situ in the field. Among the parameters, pH, temperature, EC, TDS, and DO were measured using respective probes in Lovibond meter. The turbidity of the water was measured with a turbidity meter, and a Hach salinity probe and meter were used to measure the salinity. Apart from this, a flow meter (Valeport current flow meter) was used to measure the velocity of water at all the sampling locations. The depth of velocity measurement was kept at 3–4 m (maximum reach of flow meter). All the probes and meters were calibrated before the fieldwork commenced at the laboratory.

Sample analysis

The water samples collected from 72 stations (36 samples per season) were digested using acid digestion method 3005A (USEPA 1992), where HNO_3 and HCl were used as the main reagents for digestion. This digestion was done for the analysis of ions such as Na^+, K^+, and trace metals such as Co, Cu, Mn, Pb, Zn, Se, Fe, Al, Cd, Cr, and Ba in water. The analysis of these ions and metals was carried out using Flame Atomic Absorption Spectroscopy (Perkin Elmar A Analyst 400). The concentration of major ions (Cl^-, CO_3^-, HCO_3^-, Ca^{2+}, and Mg^{2+}) and CO_2 was done using the titrimetric method (APHA 1998), whereas nutrients (SO_4^{2-}, PO_4^{3-}, NH_3, NH_4^+, NO_3^-, and NO_3-N) were analyzed in Hach DR-2800 portable Spectrophotometer using Hack test kits such as NO_3^- (cadmium reduction method), NH_3-N (salicylate method), PO_4^{3-} (ascorbic acid method), and SO_4^{2-} (sulfaVer 4 method).

Sediment samples were brought to the laboratory and dried in the oven at 60 °C. The dried samples were homogenized using a stone mortar and pestle. Meanwhile, the roots, leaves, gravels, and other anthropogenic/natural vegetable matter were removed manually. The samples were sieved for particle size analysis. The sediments collected in the pan with < 63 microns were used to perform the digestion by the Perkin Elmer Titan MPS Microwave digestion system. So, the present study reports the bulk geochemistry of the fine fraction of the sediments (< 63 μm) and their mechanisms. In the case of SS, collected 20 L water samples were stored for 2 weeks to settle the suspended solids down. Once they were settled, the upper half of the water layer was pumped out from the container using a small submersible pump without disturbing the lower half of the tank and filtration through a 0.45-μm filter paper was done using a vacuum pump. The water in the lower half of the container was subjected to a centrifuge to extract the settled suspended solids. The samples were dried at 60 °C to remove the water content and subjected to total digestion using Perkin Elmar Titan MPS Microwave Digester.

Two hundred milligrams of both the sediments and SS samples were digested using Perkins Elmar Titan MPS predefined method (Perkin 2013) with 2 mL of hydrofluoric acid (HF; 49%) and 6.6 mL of hydrochloric acid (HCl; 39%). After the digestion, 2 mL of boric acid (H_3BO_3) was added into the digested solution and heated using a hotplate to reduce the complexity of HF in the solution. The analysis for metals (Al, Cr, Mn, Fe, Co, Cu, Zn, Cd, Ba, Se, and Pb) was done using Flame Atomic Absorption Spectroscopy (Perkin Elmar A Analyst 400).

Calibration and data accuracy

For the accuracy of Perkin Elmar A Analyst 400, calibration curves were obtained first using the standards prepared from the stock and sub-stock. These standard curves were obtained before the analysis of water and sediment samples. The instrument conditions and detection limits are given in the supplementary Table 1. One preliminary analysis was also done prior to the analysis to check the limits of concentration of metals in the samples and the range was adjusted according to the need depending on the obtained results. The correlation coefficient (R^2) for each metal was determined from the calibration curve and made sure that it was above 0.995 to ensure reliable results. To ensure stability in the accuracy of results, quality check (QC) was done at every 20-sample interval throughout the analysis. Standard reference materials such as MESS-3 and BCR-701 were utilized for quality control during AAS analysis.

Data analysis

Geochemistry and statistical analysis

To understand the geochemical processes, variability and distribution of different parameter factor analysis were employed using SPSS software (version 20) for the water, floor sediments, and suspended solids separately by adapting principal component analysis (PCA) with varimax rotation. The correlated variables which were linearly related form one factor represented as a gradient (eigen vector) in multidimensional space. Varimax rotation was utilized for the analysis, where each factor is independent of the others and those with eigenvalues > 1 were considered for interpretation. In addition, PCA was utilized to transform original factor data into a form that can be evaluated in multidimensional (Euclidean) space. Additionally, to identify the water types, base exchange, and chemistry, Piper plot (Piper 1944), IBE (Schoeller 1967) and Gibbs plot (Gibbs 1970) were utilized.

Saturation index

The thermodynamic stability of estuarine water with respect to specific mineral compositions was estimated using WATEQ4F and its integrated database. Such modeling helps to identify mineral and gas mole transfers that account for differences in the composition of an initial and final water within specified compositional uncertainty limits (Ledesma-Ruiz et al. 2015). The SI can be calculated by the log-ratio value of ionic activity product in water (IAP) (Ferrer et al. 1988) with respect to the solubility product of the mineral (Ksp).

$$SI = \log\left(IAP/K_{sp}\right) \tag{1}$$

Isotopic analysis

Oxygen ($\delta^{18}O$) and deuterium (δD) isotopes were analyzed at Isotope Hydrology Division of the Center for Water Resource Development and Management (CWRDM), India, using continuous-flow isotope ratio mass spectrometry (FINNIGAN DELTA^{PLUS} XP). International isotope standards (VSMOW and GFLES-1) were used during periodical calibration of the instruments. Stable isotope values were represented by δ (expressed in terms of parts per million, ‰) and defined as

$$\delta(‰) = \left(\frac{R_{sample} - R_{std}}{R_{std}}\right) \times 10^3 \tag{2}$$

where R is D/H or $^{18}O/^{16}O$ and SMOW is the Standard Mean Ocean Water. A regression line between $\delta^{18}O$ and δD was derived from the water samples collected around the world

and referred to as Global Meteoric Water Line (GMWL) (Craig 1961). This GMWL is expressed as

$$\delta D (‰) = 8\delta^{18}O + 10 \tag{3}$$

The d-excess (excess of deuterium), which explains the connection of water to the kinetic fractionation of falling raindrops and the vapor source of regional meteorological conditions can be obtained using the equation given below (Dansgaard 1964)

$$d - excess (‰) = \delta D - 8\delta^{18}O \tag{4}$$

Partitioning of metals between particulate and dissolved phase

The partitioning of trace metals in the aquatic system can be impacted by various controlling parameters such as pH, salinity, turbidity, and amount of SS in the water column (Zhang et al. 2018; Yang and Wang 2017; Kumar et al. 2010). In such a scenario, the calculation of the partition coefficient (K_d) helps to evaluate the partitioning balance of trace metals between the particulate phase and liquid phase (Zheng et al. 2013; Zhang et al. 2018). The calculation was done for trace metals such as Co, Cu, Mn, Zn, Se, Fe, Cd, Ba, and Cr depending on their concentration in the particulate phase (Me_p) and metals/metalloids in the dissolved phase (Me_d), where Me_p is considered in mg kg^{-1} and Me_d is considered in mg L^{-1}.

$$K_d = {}^{Me_p}/_{Me_d} \tag{5}$$

K_d is represented by the distribution co-efficient and expressed in mg metal per kg. The higher value of K_d (> 3) shows the affinity of metals towards SS or absorption whereas, a lower value than 3 represents a higher affinity of metals towards liquid phase or dissolution under varying environmental conditions (Kumar et al. 2010; Zheng et al. 2013; Zhang et al. 2018; Yang and Wang 2017; Sedeño-Díaz et al. 2020).

Results and discussion

Hydrochemistry

The descriptive statistics of the parameters measured in water, sediment and SS during SWM and NEM is presented in Table 1, and the actual elemental concentrations are given in supplementary Table 2. The spatial distribution of physico-chemical parameters is given in supplementary Fig. 1. Salinity in the study area near the river mouth has the highest values during both SWM and NEM

mainly due to tidal water influence, especially at station 1 (nearest to the sea) (supplementary Fig. 2). Parameters such as EC and TDS followed a similar trend as salinity. TSS and turbidity were higher and gradually increased towards the lower reaches of the estuary during SWM, whereas these parameters found higher in the upper reaches during NEM. DO was found lesser in the lower part during SWM whereas found higher during NEM in the same region, which may be due to the higher infusion of freshwater due to high rainfall. High pH was recorded in the upper part of the estuary as compared to the lower part for both seasons. A frequent fluctuation of velocity was observed in the estuary during both seasons, and higher velocity was recorded in the lower part, which might be governed by an oscillatory gradient of tidal water during SWM due to high tide or steady gradients in subtidal water level during NEM due to low tide (Sassi and Hoitink 2013). In case of major ions, concentration of Cl^- and Na^+ are found highest in concentration during both seasons. Overall mean abundance of ions during SWM and NEM can be observed as $Cl^- > Na^+ > SO_4^{2-} > HCO_3^- > K^+ > Ca^{2+} > Mg^{2+}$ and $Cl^- > Na^+ > Mg^{2+} > Ca^{2+} > SO_4^{2-} > HCO_3^- > K^+$, respectively. Among the measured nutrients, PO_4^{3-} and NO_3 dominated the estuary during SWM and NEM. The mean abundance of nutrients can be observed as $PO_4^{3-} > NH_3 > NH_4^+ > NO_3^- > NO_3\text{-N}$ in SWM and $NO_3^- > NH_4^+ > NH_3 > NO_3\text{-N} > PO_4^{3-}$ during NEM. The dominancy of PO_4^{3-} is contributed by the saline sediments presence in the estuary and low flow of the river where terrigenous Fe (III) bounds to P deposited in the sediment while releasing PO_4^{3-} into the water column (Hartzell and Jordan 2012), whereas prevailing freshwater conditions during NEM have reduced the abundance of PO_4^{3-} in estuarine water. The concentrations of all metals during NEM were higher than SWM except for Cr, Mn, Ba, and Se. The concentrations of Se and Fe have significant dominance in the estuarine waters during both seasons. The mean dominance of metals in water can be observed as $Se > Fe > Cr > Mn > Zn > Ba > Cu > Cd > Co$ during SWM and $Fe > Se > Cu > Co > Zn > Cr > Zn > Ba > Cd = Pb$ during NEM. Similarly, Fe was found to be the dominating metal in suspended solids for both seasons, and a higher concentration of Fe is noticed during SWM, whereas vice versa condition prevailed in the case of Mn in the estuary. The absence of dissolved Al in water during both seasons and the high concentration of Al in SS indicates that it is originating from catchment areas as detrital input. In sediments, Fe and Al were the dominating metals irrespective of the seasons. The average values of both metals indicates higher concentration during SWM as compared to NEM (Table 1). The abundance of considered metals during SWM and NEM are as follows $Al > Fe > Ba > Co > Cu > Se > Mn > Zn > Cr > Pb > Cd$ and $Fe > Al > Co > Ba > Se > Cu > Mn > Zn > Cr > Cd > Pb$.

Controlling mechanisms

During SWM, all the samples fall under the Na-Cl type of water in the Piper plot and are directly influenced by seawater in the estuarine region (Fig. 3). This phenomenon can be explained by the variety of conditions like gentle coastal hydraulic gradients, tidal and estuarine activity, sea level rises, low infiltration, excessive withdrawal, and local hydrogeological conditions (Sivasubramanian et al. 2013; Senthilkumar et al. 2017). In this study, the Na-Cl type of water is dominating because of the high tidal influence, considering the time of sample collection along with the low flow of the Sibuti River system due to less rainfall during the SWM period. However, in the diagrams for NEM, samples fall under various facies including Na-Cl type, Ca–Cl type, and Ca–Mg–Cl type, unlike the SWM. The dominant water type in NEM can be represented as Ca–Cl type > Na-Cl type > Ca–Mg–Cl type (Fig. 3). Samples falling in the Ca–Cl type are prominent at the most upstream side of the estuary, which indicates the weathering of limestones and dolomites in the catchment areas or direct recharge from rainwater. During the phase of seawater intrusion, underneath the freshwater flow, there is an initial increase in salinity and a rapid and marked reverse exchange of Na/Ca, which is recognized by the characteristic Ca–Mg–Cl facies (Ravikumar and Somashekar 2017). This type of water evolves towards facies that are closer to seawater (Na-Cl). This coastal region possibly represents ion-exchange reactions or a hydrochemical evolutionary path from Ca–Cl and Ca–Mg–Cl water type to Na–Cl water type. Similar observations were confirmed by indices of base exchange, where 30 samples showed an indication of base ion exchange in water, whereas 6 samples in the same condition showed reverse ion exchange. On the contrary, during NEM, this process is opposite and showed 33 samples under exchange between Na^+ and K^+ in water with Mg^{2+} or Ca^{2+} in rock and is an indication of reverse ion exchange. Considering the sharp increase in the concentration of Ca^{2+} and Mg^{2+} during NEM, it is an indication of the mixing of various weathered ions in river water through runoff from its catchment, which mainly consists of sandstones and calcareous sandstone, shale, limestone, and marl and are dominant in Sibuti and Lambir formations (Nagarajan et al. 2015, 2017a). These rocks are prominent to weathering and consist of calcite ($CaCO_3$), dolomite ($CaMg (CO_3)$), and less prominent feldspars along with weathering resistant minerals like quartz (Nagarajan et al. 2015; Simon et al. 2014). On the other hand, the increase in the concentration of Cl^- from SWM to NEM is also attributed towards the base exchange of Na^+ for Ca^{2+} and Mg^{2+} as mentioned earlier.

Samples in Gibbs plot indicated an integrated mechanism of high weathering, low evaporation, and precipitation along with input from other sources (Annapoorna and Janardhana 2015). These sources might include the effect

Table 1 Descriptive statistics of elemental concentrations in water, suspended solids, and sediments, including isotopes in water

Parameters	Units	SWM				NEM			
		Min	Max	Mean	St. Dev	Min	Max	Mean	St. Dev
Physico-chemical parameters									
pH	-	4.6	6.88	6.16	0.33	5.45	7.6	6.61	0.4
DO	mg L^{-1}	3.66	6.44	4.44	0.44	13.2	35.1	20.49	5.15
EC	µS cm^{-1}	107.6	3170	409.6	719.63	139.59	11,971.44	1707.25	2805.01
TDS	mg L^{-1}	153.8	4528.6	585.15	1028.05	97.71	8380.01	1195.08	1963.51
Turbidity	NTU	7.87	53.9	27.9	9.61	15.1	50.1	31.69	8.37
Velocity	m/s	0.7	11.84	3.58	2.02	0.29	2	0.88	0.48
Salinity	ppt	0.02	1.65	0.61	0.59	0.04	11.7	1.05	2.12
Temp	°C	21.4	30	28.4	1.39	29.8	32	30.04	0.44
CO_2	mg L^{-1}	4.4	15.4	6.91	2.42	11	39.6	20.96	5.84
TSS	mg L^{-1}	20.2	178.6	55.62	39.3	44	384.3	156.81	92.33
Major ion concentrations in water									
Ca^{2+}	mg L^{-1}	2	14	4.83	3.1	2	286	60.58	67.59
Mg^{2+}	mg L^{-1}	BDL	54	4.7	9.47	BDL	1082.4	125.92	233.3
Na^+	mg L^{-1}	20.4	1252.8	134.7	261.2	2.76	3034	292.97	582.29
K^+	mg L^{-1}	7.96	75.05	15.89	13.1	2.88	98.26	17.1	16.3
HCO_3^-	mg L^{-1}	18.3	54.9	31.35	7.46	12.2	61	27.45	10
Cl^-	mg L^{-1}	26.58	2153.58	182.17	441.71	17.72	5742.9	621.85	1131.22
SO_4^{2-}	mg L^{-1}	6	89	34.97	20.35	2	133	46.86	45.05
Nutrient concentrations in water									
PO_4^{3-}	mg L^{-1}	BDL	3.45	0.87	0.92	0.03	0.35	0.11	0.06
NO_3-N	mg L^{-1}	BDL	0.08	0.03	0.02	BDL	0.86	0.19	0.32
NH_3	mg L^{-1}	0.01	0.9	0.18	0.23	0.17	0.97	0.58	0.21
NH_4^+	mg L^{-1}	0.04	0.32	0.15	0.07	0.18	1.03	0.61	0.22
NO_3^-	mg L^{-1}	0.01	0.34	0.12	0.07	BDL	4.09	0.85	1.43
Stable isotopes in water									
δD	$^0/_{00}$	− 85.41	− 72.55	− 79.88	5.54	− 59.06	− 41.89	− 48.99	7.16
$δ^{18}O$	$^0/_{00}$	− 11.20	− 9.80	− 10.67	0.56	− 11.02	− 5.74	− 7.64	1.1
d-excess	$^0/_{00}$	0.83	8.25	5.47	2.78	2.89	29.10	12.15	10.75
Metal concentrations in water									
Cu	mg L^{-1}	BDL	0.386	0.036	0.089	0.178	0.556	0.293	0.068
Zn	mg L^{-1}	BDL	0.534	0.109	0.102	0.015	1.065	0.151	0.189
Fe	mg L^{-1}	1.375	3.950	2.294	0.556	0.240	67.480	6.507	11.348
Co	mg L^{-1}	BDL	0.046	0.003	0.009	0.179	0.351	0.261	0.063
Mn	mg L^{-1}	0.096	0.306	0.164	0.052	BDL	0.238	0.042	0.047
Cd	mg L^{-1}	0.016	0.077	0.026	0.011	BDL	0.025	0.003	0.005
Pb	mg L^{-1}	BDL	BDL	BDL	BDL	BDL	0.097	0.003	0.016
Cr	mg L^{-1}	0.007	0.541	0.324	0.136	BDL	0.424	0.118	0.135
Se	mg L^{-1}	3.445	8.559	6.236	1.153	2.784	6.47	5.522	0.640
Ba	mg L^{-1}	BDL	0.996	0.074	0.199	BDL	0.536	0.031	0.102
Metal concentrations in suspended solids									
Co	mg kg^{-1}	651	1650	1145.4	426.5	1287	2389	1879.6	416.5
Cu	mg kg^{-1}	752.3	1545	1026.6	322.3	187.6	854.2	548.6	315
Mn	mg kg^{-1}	785.5	1573	1158.8	386.7	1730	2902.5	2321.8	503.5
Zn	mg kg^{-1}	158.5	279.5	232.6	60	111.5	188.5	141.3	30.7
Se	mg kg^{-1}	86	436	225.7	142.4	14	293	212.4	112.8
Fe	mg kg^{-1}	33,430	46,890	38,244	5291.8	23,340	37,610	29,116	6054.7
Al	mg kg^{-1}	17,310	21,045	19,282	1609.6	4335.5	10,670	7645.1	2533.2

Table 1 (continued)

Parameters	Units	SWM				NEM			
		Min	Max	Mean	St. Dev	Min	Max	Mean	St. Dev
Cd	mg kg^{-1}	4.7	12.75	6.68	3.45	3.55	6.15	4.34	1.1
Ba	mg kg^{-1}	507.5	279.5	826.4	502.6	563	1601.5	1059.8	452.1
Metal concentrations in sediments									
Co	mg kg^{-1}	796.5	2337.2	1318.11	355.27	1331.4	2902.9	1969.36	419.82
Cu	mg kg^{-1}	76.8	3901.3	1050.78	764.46	134	952.9	355.67	224.93
Mn	mg kg^{-1}	38.7	523.3	174.19	118.31	39	399.30	163.23	89.51
Pb	mg kg^{-1}	BDL	11.4	3.35	3.36	BDL	0.2	0.01	0.03
Zn	mg kg^{-1}	86.4	213.5	133.97	31.91	91.6	197	127.59	30.48
Se	mg kg^{-1}	527.7	1081.1	789.87	138.36	494.3	931.6	744.01	112.78
Fe	mg kg^{-1}	33,205.7	90,397.5	52,496.3	15,269.24	27,673.6	65,400.8	39,527.7	10,870.18
Al	mg kg^{-1}	16,651.5	227,258.1	110,824.88	54,123.51	1862.4	102,302	27,635.87	33,237.45
Cd	mg kg^{-1}	0.99	1.74	1.25	0.19	0.96	1.53	1.18	0.14
Cr	mg kg^{-1}	29.7	113.8	92.63	22.99	99.3	113.3	110.96	2.15
Ba	mg kg^{-1}	774.1	7511.3	2301.48	1569.24	210.3	3186	1487.73	848.29

BDL, below detection limit

of seawater intrusion because of the tides along with the agricultural run-off, during SWM . In contrast, NEM has shown a major variation in the plot by the representation of samples in weathering zone due to rock-water interaction and also in evaporation zone. The majority of the samples in the cation plot falls in the rock weathering field, which may be due to the weathering in the upstream and downstream regions of the river as discussed earlier. On the contrary, the rest of the cations and all the anions fall outside the defined zone (Fig. 4), indicating an additional anthropogenic similar mechanism during SWM.

Saturation index (SI)

In both seasons, carbonate, sulfate, and halide groups of minerals were found to be in undersaturated condition in the estuary except for oxide and oxyhydroxide group of minerals such as magnetite and goethite, which were found to be in over saturated condition during SWM (Fig. 5). The log pCO_2 was found higher than the atmospheric equilibrium (−3.5) (Prasanna et al. 2010; Srinivasamoorthy et al. 2014). In such a case, respiration of organic matter and dissolution of carbonate minerals play a major role in the increase of CO_2. Meanwhile, pH in the estuary is inversely related to log pCO_2. These values indicate a higher residence time of river water during SWM due to the low flow of the river, whereas lower log pCO_2 values during NEM are an indication of the freshwater recharge because of higher rainfall during this monsoon. The absence of any definite trend of EC with carbonate (calcite, magnesite, aragonite, and dolomite) and sulfate minerals (gypsum and anhydrite) (Fig. 5) suggests the negligible influence of seawater in the dissolution of

these minerals. The higher dissolution of carbonates is due to the higher residence time of water coupled with degassing of CO_2 (Chidambaram et al. 2011) in water. This was confirmed by an observed lower average value of log pCO_2 during SWM. The dissolution of sulfate minerals was found to be more aligned and falling along the recharge line of the river during NEM (Fig. 5). Higher fresh recharge, higher discharge, abundance of TSS, higher pH, and lower log pCO_2 in the upper part are also responsible for higher dissolution of sulfate minerals during NEM. The dissolution is highest for halite than any other minerals considered in the current study, which may be due to its nature of high solubility (Klimchouk et al. 1996; Naderi et al. 2016). It responds to EC during both seasons perfectly with dissolution decreases with higher EC values. During SWM, higher dissolution takes place between 100 and 200 μS/cm of EC, whereas dissolution is well spread during NEM due to reducing saline water influence through freshwater recharge. On the other hand, SI values of halite relate significantly with log pCO_2 and pH during NEM, indicating a lower residence time of saline water (Prasanna et al. 2010; Naderi et al. 2016) while an increase in dissolution in the seawater flow direction (towards upstream direction). This is due to the intensive mixing and ion exchange process caused by the dissolution of gypsum and anhydrite (Hamzaoui-Azaza et al. 2013; Juen et al. 2015; Naderi et al. 2016) and validates the Ca–Mg–Cl type of water observed during NEM, whereas the domination of Na-Cl type of water ruled out such ion exchange processes (Juen et al. 2015). Fe oxides are found to be precipitating during SWM, whereas such precipitation/dissolution is uncommon in NEM water samples. These oxides show an increasing trend with an increase in pH and a decrease in log

Fig. 3 Piper plot representation
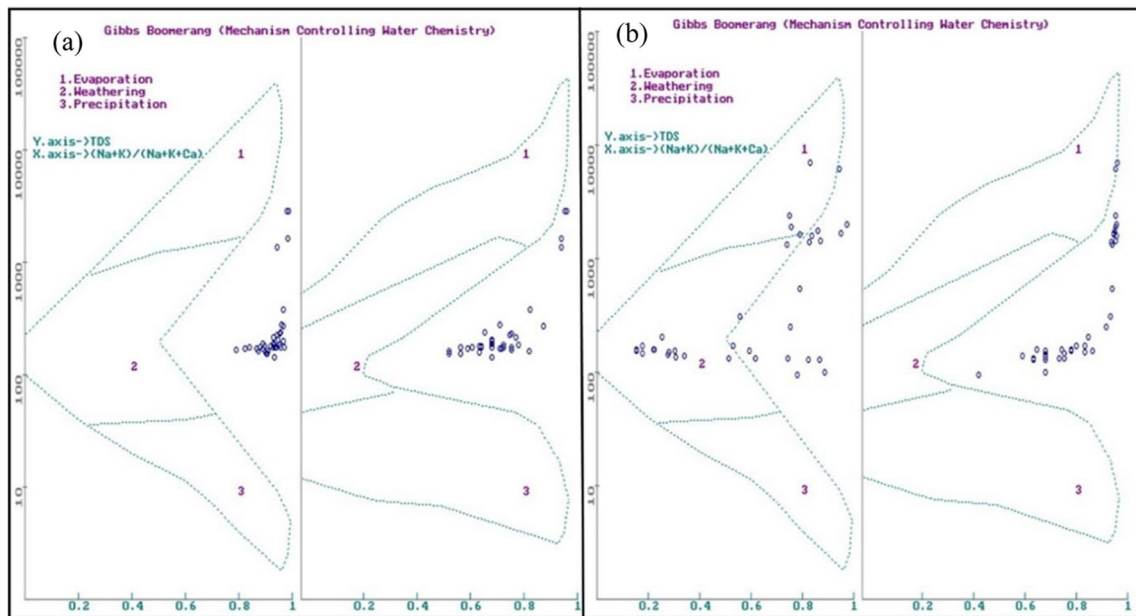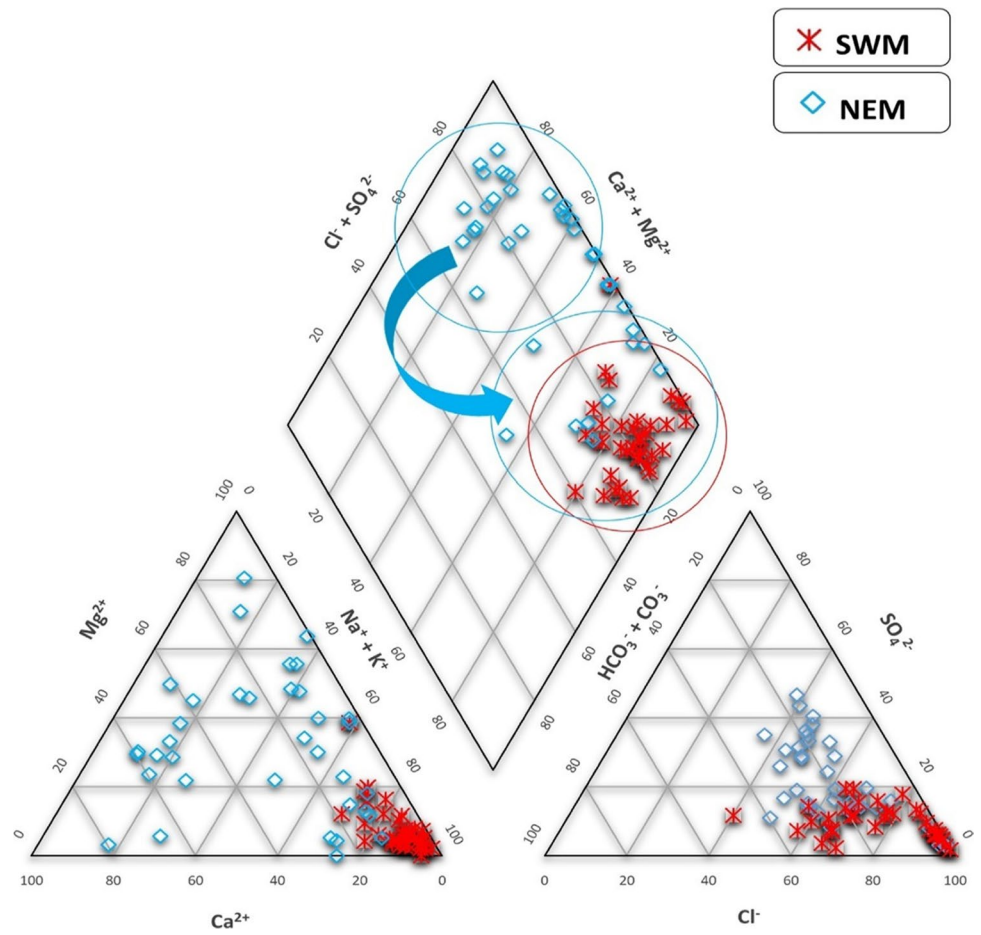of water during SWM and NEM

Fig. 4 Gibbs classification of water samples according to mechanisms controlling the water chemistry during SWM (a) and NEM (b)
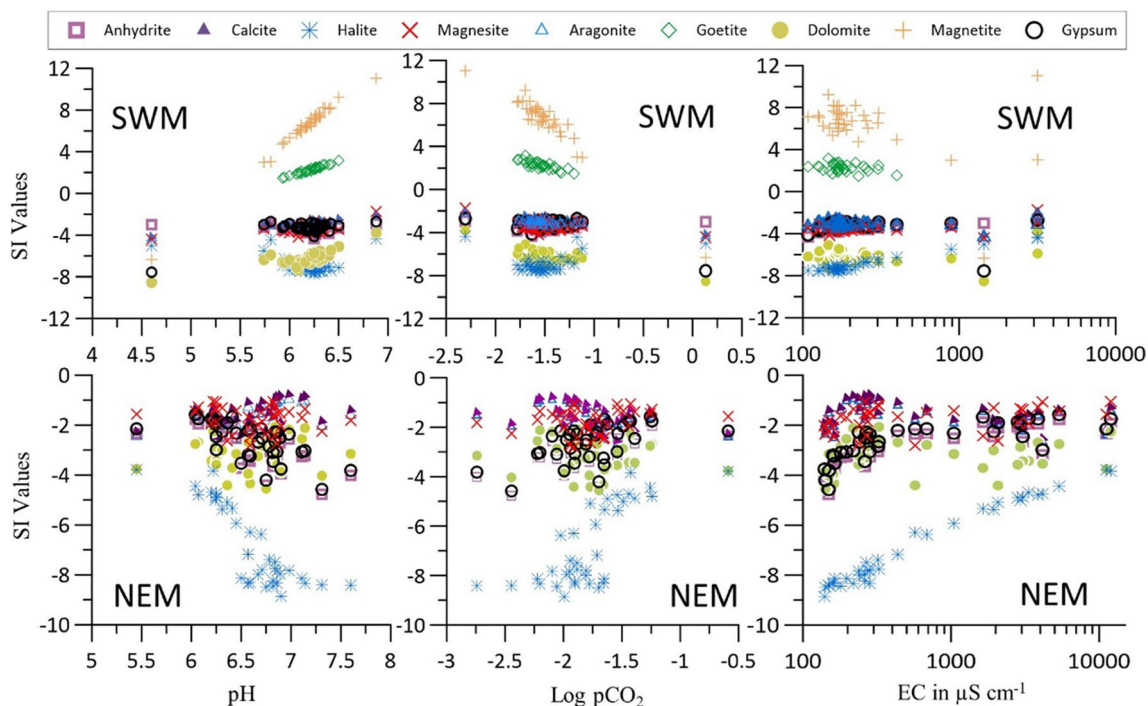
Fig. 5 Relationship of log pCO_2, pH, and EC with SI of minerals

pCO_2 values of water in the estuary (Fig. 5). The supersaturation state of magnetite is responsible for lowering the concentration of dissolved Fe in estuarine water. Both oxide and oxyhydroxides approach saturation with a decrease in pH condition, attributed to the changes in redox conditions, pH, and hydrolysis reactions (Mapoma et al. 2017). According to Tosca et al. (2019), effluent-seawater mixing with river water strongly reduces the flux of dissolved Fe into the sea due to the formation of oxides and oxyhydroxides. These observations suggest that the precipitation of Fe is mainly associated with the residence time of river water for a longer period during SWM as compared to NEM (Fig. 5). This might be due to increased tidal resistance observed in the river and low flow (seasonal fluctuation) which is allowing Fe to precipitate (Mapoma et al. 2017) in the estuary in the form of magnetite and goethite.

Statistical evaluation

Factor analysis was carried out for all the parameters in water, sediments, and suspended solids for both seasons to identify the underlying geochemical processes and sources. The varimax rotation utilized for factor analysis for both seasons and the rotated component matrix is presented in Tables 2 and 3 for water, Table 4 for SS, and Tables 5 and 6 for sediments. The components having eigen values > 1 were considered for interpretation. The factor analysis for water explained 82.27 and 82.95% of variance during SWM and NEM (Tables 2 and

3), respectively, and the factor analysis for suspended solids explained 95.17 and 93.62% of variance (Table 3) for both seasons. Similarly, factor analysis carried out for sediments explained 72.65 and 72.87% of the variance (Tables 5 and 6).

Geochemical mechanisms in water

Southwest monsoon (SWM) The 8 factors during SWM with eigenvalues more than one were considered. Factor 1 has major EC, TDS, velocity, Cl^-, Mg^{2+}, Ca^{2+}, Na^+, K^+, SO_4^{2-}, NH_4^+, and Ba. This factor has a major association at station 1 with a factor score of 4.383 (Fig. 6a). The association and trend of these parameters in water indicate the domination of seawater in the estuary during SWM (Patra et al. 2012). Factor 2 is loaded with turbidity, salinity, TSS, Fe, and Mn, where a negative loading of DO, Se, and Cr is also associated with the process (Fig. 7c). This indicates the tidal-induced turbidity in the estuary initiating resuspension of suspended solids (Uncles et al. 1985) and reveals the injection of Fe and Mn into the water column from the hydroxide phases available in the sediments and suspended solids (Turner and Millward 2000; Callaway et al. 1988). This factor is dominant in the mid zones of the estuary (stations 6 to 13; Fig. 8a) and the association of TSS indicates particulate organic matter association of sediments and suspended solids with the formation of cation-induced coagulation of negatively charged humic colloids containing Fe and Mn in this zone. This forms organic Fe and Mn complexes

in a water solution with a reduction of DO in water (Shapiro 1964; Sholkovitz 1976; Boyle et al. 1977; Mayer1982; Zhou et al. 2003; Jilbert et al. 2016; Wen et al. 2019) and might be responsible for absorption of Se and Cr from the water column (Bewers and Yeats 1978; Campbell and Yeats 1984). The positive loading of pH with negative loading of CO_2 and Ba in factor 3 indicates the reaction of CO_2 with seawater to cause respiration of organic matter with the generation of various organic acids including the formation of carbonic acid in water, making the water acidic (Eq. 6) (Mook and Koene 1975; Mucci et al. 2011; Saifullah et al. 2014; Van Dam and Wang 2019).

$$H_2O + CO_2 \iff H_2CO_3(\text{carbonic acid}) \iff H^+ + HCO_3^- \tag{6}$$
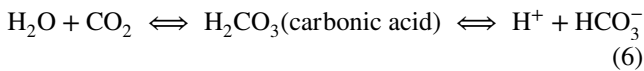
NO_3^- and NO_3-N loading in factor 4 and high factor scores near stations 6, 23, 24, 25, and 26 (Fig. 6a), which are near various agricultural channels and tributaries such as Sungai Kejapil indicate towards the leaching of these nutrients from the adjacent agricultural and anaerobic denitrification processes in the estuary (Haaijer et al. 2006). On the other hand, factor 7 represents NH_3 with a weak negative loading DO which is an indication of the combined effect of ammonification and NO_3 reduction to NH_4^+, where DON (dissolved organic nitrogen) and NO_3 give rise to NH_4^+ (Scott et al. 1999). This process is continuing to form NH_3 with the consumption of available DO in the water column (Müller et al. 2018). The major loading of chalcophile metals such as Cu and Zn in factor 5 is mainly associated with the oxidation of pyrites (Anandkumar et al. 2022), which are widely available in Sibuti and Lambir formations (Nagarajan et al. 2015, 2017a). These metals are not associated with any physico-chemical parameters indicating the release of such metal from the source rocks due to chemical weathering. Factor 6 is loaded with PO_4^{3-} and weak loading of SO_4^{2-} and has high factor scores at stations nearer to agricultural fields (station nos.: 7, 17, 20, 26, 34, and 36) (Fig. 7a) indicating PO_4^{3-} input from agricultural runoff water (whereas prevailing freshwater Hartzell and Jordan 2012; Nystrand et al. 2016). Station 26 reported a higher loadings for both factors 4 and 6 along with a decrease in DO concentration at this station (highest DO was reported at the station 27) (Fig. 7a). This observation and weak loading of SO_4^{2-} in this factor indicate the process of denitrification coupled to sulfide oxidation and organic matter respiration with consumption of DO at station 26. This process leads to an increase in PO_4^{3-} mobilization (e.g., Lamers et al. 2002; Boomer and Bedford 2008). Factor 8 has major loading of Cd along with negative loading of HCO_3^-. Despite being a chalcophile group of elements, independent behaviour of the metal in this component indicates the leaching of Cd from agricultural fields as phosphate-based fertilizers are widely used in agricultural fields and are the major source of Cd in Malaysian rivers (De Boo 1990). This practice is common in Borneo where these fertilizers provide maximum growth to palm oil plantations in peat-based soil (Zaharah et al. 2014). The factor score for this component is higher at stations 13, 14, 26, and 36 (Fig. 7a). Considering the land use map (Fig. 2), the proximity of these stations (13, 14, and 36) is very close to the agricultural fields situated near the estuary, which further validates the source of such metal in estuarine water.

Northeast monsoon (NEM) The factor analytical results of water from NEM are summarized in Table 3 and consist of 6 major components. Factor 1 is during NEM has major loading of EC, TDS, DO, salinity, HCO_3^-, Cl^-, Mg^{2+}, Ca^{2+}, K^+, SO_4^{2-}, Cd, Ba, and Cr along with negative loading of pH (Fig. 7b). The association of the mentioned parameters indicates saline water-influenced processes like SWM despite the large infusion of freshwater during NEM from the riverine side. The factor scores of 5.36 and 1.62 at stations 1 and 2 (Fig. 7b) reveal the direct influence of seawater in the lower part of the estuary. The loading of HCO_3^- with Cl^-, Mg^{2+}, and Ca^{2+} is illustrative of their contribution from seawater as HCO_3^- presence in natural water varies from pH 4.5 to 8.3, and the dissolution of these ions is ensured by the acidic condition near the mouth and indicated by negative pH loading. Positive loading of Cd and Ba attributes to the immediate increase in salinity near the mouth and is giving rise to the concentration of Ba (Coffey et al. 1997) and Cd (Greger et al. 1995) from the suspended particles and sediments. Factor 2 has major loading of EC, TDS, Mg^{2+}, Cl^-, Ca^{2+}, SO_4^{2-}, and NO_3^- and has a negative affinity towards pH, Co, Cr, and turbidity, which contributes 20.27% of the total variance. This factor indicates the intense mixing of fresh water in the lower region of the estuary, where high factor scores observed from stations 2 to 9 (Fig. 7b) have a higher affinity with this component. The association of EC, TDS, Mg^{2+}, Cl^-, and Ca^{2+} indicates towards ion exchange process (Thivya et al. 2015) in the estuary (Fig. 7d). Regarding negative loading of Co and Cr and turbidity, these metals are removed from the water column and finding their way to the sediments with an increase in the influence of Cl^- (seawater). Under such conditions, Cr forms a hexaaquo complex ($[Cr(H_2O)_6]Cl_3$). These hexaaquo complex and Cr-organic associations are stable in freshwater but destabilize with an increase in ionic strength and precipitate as floccules (Pađan et al. 2019; Campbell and Yeats 1984). Due to the intensive mixing, DO carried by river water plays a major role in the positive loading of both SO_4^{2-} and NO_3^-. Sulfides under reoxygenated conditions are oxidizing to sulfates and remineralization of organic matter gives rise to more SO_4^{2-} in the water column (Patra et al. 2012; Matson and Brinson 1985; Malcolm et al. 1986). In addition, the nitrification

process (nitrogen cycle) increases with the availability of DO to produce more NO_3 in the water column from NH_3 and NH_4^+. Such a process gives rise to more H^+ ions and acidic conditions in water, which justifies the negative loading of pH in factor 2 (Müller et al. 2018; Scott et al. 1999). The negative loading of NH_3 and NH_4^+ in factor 4 validates this reaction (Eq. 7), and high positive loading of DO is observed at the same stations while representing 9.14% in variance.

$$NH_3 + H_2O + 2O_2 \iff NH_4^+ + OH^- + 2O_2 \iff NO_3^- + 2H_2O + H^+ \qquad (7)$$
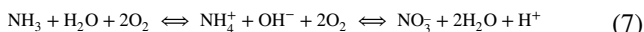
As NH_3 and NH_4^+ are the by-products of the degradation of organic matter under anaerobic conditions (Canfield et al. 1993; Baric et al. 2002), an increase in DO eliminates the enrichment of NH_3 and NH_4^+ in the estuary. The factor scores at stations 9 (2.001) and 29 (2.162) (Fig. 7b) suggest that nitrification (nitrogen cycle) is a dominating process during NEM mainly in the upper part and mixing zone of the estuary. Factor 3 has positive loading of Fe, Mn, and Zn, and the independency of this parameters with pH attributes towards the source of these metal association to be terrestrial in origin and the run-off might be the carrier of these metals during NEM as terrestrial input. As the metal association is mainly composed of chalcophile elements, oxidation of pyrites might be the major source of these metals in estuarine waters (Galán et al. 2003; Lu et al. 2005; Nieto et al. 2007; Fernandez and Borrok 2009; Chopard et al. 2017). The higher factor scores in the upper part of the estuary (station 32) (Fig. 7b) imply that the source is mainly from the Sibuti Formation, where pyrite concretions are common (Nagarajan et al. 2015, 2017a). On the other hand, higher run-off during NEM does not permit the saline water to impact the association in the upper part of the estuary. Factor 5 is loaded positively with temperature, TSS, and velocity along with high negative loading of PO_4^{3-}. PO_4^{3-} remobilization in estuary mainly

Table 2 Rotated component matrix of water contained physico-chemical parameters, major ions, nutrients, and trace metals during SWM

Parameters	Communalities	Components							
		1	2	3	4	5	6	7	8
pH	0.862	-0.049	-0.254	0.837	0.033	-0.004	0.272	-0.079	-0.110
DO	0.649	-0.145	-0.593	0.131	-0.011	-0.243	-0.093	-0.435	-0.050
EC	0.964	0.956	0.179	-0.064	-0.076	0.075	-0.053	-0.025	0.001
TDS	0.964	0.956	0.179	-0.064	-0.076	0.075	-0.053	-0.025	0.001
Turbidity	0.761	0.146	0.831	0.057	-0.109	0.029	-0.036	-0.166	-0.062
Velocity	0.693	0.438	-0.025	0.530	-0.068	0.006	-0.056	0.423	-0.182
Salinity	0.843	0.287	0.732	-0.047	-0.033	0.119	-0.325	0.278	0.155
Temperature	0.872	-0.660	-0.274	-0.553	-0.067	0.036	-0.101	-0.196	-0.002
TSS	0.708	-0.392	0.601	0.396	-0.077	-0.118	-0.026	0.077	-0.104
HCO_3	0.563	-0.110	0.130	0.319	0.041	0.174	-0.014	0.064	-0.629
Cl^-	0.898	0.914	0.152	-0.062	-0.133	0.076	-0.058	-0.087	0.002
Mg^{2+}	0.955	0.935	0.098	0.251	-0.004	0.076	-0.012	0.059	-0.010
Na^+	0.958	0.946	0.209	-0.077	0.013	0.061	-0.081	0.059	0.015
K^+	0.928	0.941	0.174	0.073	0.007	0.016	-0.064	-0.037	-0.040
Ca^{2+}	0.859	0.819	0.110	-0.191	-0.183	0.250	-0.167	0.059	-0.110
CO_2	0.809	0.251	-0.144	-0.775	-0.193	-0.018	0.178	0.136	0.194
SO_4^{2-}	0.815	0.698	0.113	-0.191	0.068	0.064	0.477	0.189	0.081
PO_4^{3-}	0.876	-0.231	-0.096	0.088	-0.154	0.012	0.879	0.088	0.052
NO_3-N	0.981	-0.095	-0.055	0.043	0.981	0.003	-0.062	-0.041	0.010
NH_3	0.581	-0.014	0.091	-0.033	-0.080	-0.076	0.069	0.743	-0.046
NH_4^+	0.687	0.590	0.274	-0.155	-0.113	0.145	-0.341	0.264	0.141
NO_3^-	0.984	-0.101	-0.080	0.100	0.972	-0.025	-0.050	-0.073	0.066
Cu	0.757	0.274	0.220	0.244	0.103	0.705	-0.033	-0.255	0.000
Zn	0.840	0.145	-0.090	-0.105	-0.086	0.881	0.024	0.085	-0.094
Fe	0.889	0.380	0.748	0.283	0.015	-0.147	0.112	0.261	0.034
Mn	0.800	0.207	0.855	-0.079	0.026	0.035	-0.043	0.114	0.051
Cd	0.819	-0.112	0.135	-0.019	0.100	0.035	0.027	-0.009	0.881
Cr	0.689	-0.519	-0.523	0.013	0.231	-0.048	0.282	0.086	-0.056
Se	0.754	-0.169	-0.643	0.399	0.076	0.193	-0.040	0.251	0.213
Ba	0.810	0.657	0.311	-0.518	0.032	-0.015	-0.013	0.109	-0.007
Percentage Variance Explained		30.179	14.499	9.658	7.476	5.391	5.195	5.066	4.812
Total Variance Explained		82.27%							
Eigen Value		Greater than 1							

Blue cells: positive factor loading; grey cells: negative factor loading

Table 3 Rotated component matrix of water contained physico-chemical parameters, major ions, nutrients, and trace metals during NEM

Parameters	Extraction	Component					
		1	2	3	4	5	6
pH	0.803	-0.588	-0.631	0.090	0.212	0.078	-0.030
DO	0.681	0.533	0.101	0.043	0.528	0.322	-0.063
EC	0.946	0.784	0.531	0.017	0.018	0.215	0.011
TDS	0.946	0.784	0.531	0.017	0.018	0.215	0.011
Turbidity	0.910	0.105	-0.832	0.189	0.273	-0.120	0.293
Velocity	0.404	0.346	0.030	0.003	-0.014	0.506	0.156
Salinity	0.963	0.936	0.300	-0.001	-0.039	0.074	0.055
Temperature	0.463	0.293	0.117	-0.009	0.135	0.585	-0.087
TSS	0.769	0.291	-0.059	0.423	0.225	0.578	-0.046
HCO_3	0.806	0.626	-0.055	-0.012	0.193	0.344	0.499
Cl^-	0.832	0.658	0.574	0.010	0.054	0.257	-0.007
Mg^{2+}	0.893	0.822	0.407	0.084	-0.058	0.203	0.042
Na^+	0.975	0.911	0.376	-0.004	-0.008	0.101	0.038
K^+	0.943	0.913	-0.045	0.030	0.237	0.211	0.091
Ca^{2+}	0.732	0.458	0.606	0.086	-0.098	0.305	-0.217
CO_2	0.449	-0.171	-0.442	0.125	-0.288	0.327	-0.134
SO_4^{2-}	0.971	0.462	0.850	-0.014	-0.151	-0.037	0.103
PO_4^{3-}	0.603	-0.160	-0.134	0.134	0.000	-0.719	0.101
NO_3-N	0.882	0.330	0.808	0.055	0.138	0.231	0.218
NH_3	0.916	0.060	0.146	0.008	-0.935	-0.009	0.088
NH_4^+	0.917	0.066	0.154	0.012	-0.934	-0.002	0.087
NO_3^-	0.877	0.321	0.803	0.048	0.129	0.223	0.251
Cu	0.756	0.430	-0.111	-0.237	0.236	-0.364	-0.559
Zn	0.935	0.047	-0.097	0.951	0.004	-0.131	-0.049
Fe	0.950	-0.074	-0.141	0.959	0.013	-0.047	0.039
Co	0.845	-0.176	-0.805	0.113	0.382	0.015	0.030
Mn	0.891	0.084	0.061	0.934	0.002	0.065	-0.037
Cd	0.972	0.879	0.437	0.022	-0.028	0.090	-0.054
Cr	0.733	0.354	-0.564	0.240	0.430	0.104	0.130
Se	0.883	-0.125	-0.052	0.135	0.164	0.267	-0.866
Ba	0.923	0.944	0.115	0.009	-0.023	0.159	-0.035
Percentage Variance Explained		31.510	20.270	9.495	9.140	7.092	5.445
Total Variance Explained		82.951%					
Eigen Value		Greater than 1					

Blue cells: positive factor loading; grey cells: negative factor loading

happens under reducing conditions (Deborde et al. 2007). The absorption of PO_4^{3-} by sediments happens under an increase in temperature with decreasing salinity conditions (Zhang and Huang 2011). During NEM, infusion of freshwater rich in DO decreases the reducing conditions, whereas resistance provided by such freshwater input towards saline water input can be validated by positive loading of velocity from the riverine side. Positive loading of temperature and negative loading of PO_4^{3-} indicate the sorption of PO_4^{3-} under such conditions where it is finding its way to suspended solids and sediments. The factor scores suggest this process to be dominant in the upper part of the estuary. On the contrary, stations 2 and 4 are observed to have higher factor scores (Fig. 7b), which is mainly because of the higher turbidity

and concentration of DO observed in these stations. Factor 6 has positive loading of HCO_3^- and negative loading of Cu and Se. The negative loading of Cu might be due to the formation of insoluble $[Cu (HCO_3)_2]$ and association with organic compounds that exist in colloidal form favored by an increase in HCO_3^- concentration in water (Drogowska et al. 1994; Namieśnik and Rabajczyk 2010) while removing it from the water column. Similarly, under well-oxygenated conditions, sorption of the dissolved form of Se such as SeO_3^{2-} and SeO_4^{2-} on sediments and suspended solid happens in aqueous conditions (Kieliszek 2019; Hung and Shy 1995), and such retention is closely linked with the presence of organic matter in water (Söderlund et al. 2016). This process is dominant in the lower part of the estuary (Fig. 7b).

Table 4 Rotated component matrix of trace metals in SS during SWM and NEM

Parameters	SWM				NEM			
	Communalities	Component			Communalities	Component		
		1	2	3		1	2	3
pH	0.991	-0.921	0.196	0.324	1.000	0.965	0.025	0.262
DO	0.946	-0.940	0.150	-0.198	0.943	-0.038	0.952	-0.190
Turbidity	0.997	0.981	-0.165	-0.084	0.993	0.938	0.314	0.118
Salinity	1.000	0.939	-0.342	-0.043	0.999	-0.961	0.263	0.080
TSS	0.975	0.945	-0.179	-0.225	0.700	-0.189	0.598	0.554
Co	0.917	-0.323	0.260	0.863	0.939	0.541	0.764	0.251
Cu	0.992	0.979	-0.102	-0.151	0.988	-0.818	-0.557	-0.095
Mn	0.996	0.585	-0.549	-0.740	1.000	-0.642	-0.715	-0.278
Zn	0.930	0.540	-0.756	-0.258	0.999	-0.990	-0.110	-0.085
Se	0.992	-0.546	0.832	-0.034	0.982	0.939	0.170	-0.266
Fe	0.999	-0.045	0.989	-0.141	0.994	0.023	-0.187	0.979
Al	0.984	-0.699	-0.602	0.365	0.995	0.909	0.336	-0.238
Cd	0.855	0.207	-0.395	0.810	0.576	-0.045	-0.318	-0.687
Ba	0.748	-0.091	0.829	0.228	0.997	0.611	0.718	0.330
Percentage Variance Explained		48.65	29.04	17.5		51.49	26.02	16.11
Total Variance Explained		95.17%				93.62%		
Eigen Value		Greater than 1				Greater than 1		

Blue cells: positive factor loading; grey cells: negative factor loading

Table 5 Rotated component matrix of metals in sediments during SWM

Parameters	Communalities	Component				
		1	2	3	4	5
pH	0.766	-0.234	0.040	0.754	0.357	0.120
DO	0.564	-0.732	0.000	-0.067	0.069	0.136
Salinity	0.760	0.822	0.086	-0.071	-0.171	0.205
TSS	0.729	0.809	-0.232	0.014	-0.109	0.098
Turbidity	0.846	0.725	-0.222	-0.217	0.115	0.460
Co	0.874	-0.119	-0.251	0.038	0.891	-0.032
Cu	0.554	0.335	0.316	-0.438	-0.261	0.287
Mn	0.614	0.035	-0.108	0.045	0.182	-0.752
Pb	0.809	0.816	-0.103	-0.116	-0.319	0.129
Zn	0.857	-0.267	0.876	-0.134	-0.016	0.026
Se	0.749	0.752	0.085	-0.334	-0.218	0.129
Fe	0.501	0.570	0.323	0.141	0.114	-0.195
Al	0.807	0.128	0.868	-0.101	-0.152	0.059
Cd	0.600	0.141	-0.016	0.199	-0.028	0.734
Cr	0.898	0.116	-0.215	0.900	-0.138	0.094
Ba	0.695	-0.265	0.099	0.140	0.673	-0.378
Percentage of Variance Explained		27.015	12.411	11.648	10.881	10.695
Total Variance Explained		72.651%				
Eigen Value		Greater than 1				

Blue cells: positive factor loading; grey cells: negative factor loading

Table 6 Rotated component matrix of metals in sediments during NEM

Parameters	Communalities	Components				
		1	2	3	4	5
pH	0.851	-0.631	-0.639	0.149	-0.047	0.142
DO	0.615	-0.058	0.687	0.318	0.118	0.156
Salinity	0.952	0.246	0.935	-0.099	-0.071	0.050
TSS	0.743	-0.166	0.329	0.225	0.028	0.746
Turbidity	0.684	-0.788	0.012	0.060	-0.214	0.121
Co	0.711	-0.324	0.152	0.314	-0.111	-0.687
Cu	0.581	0.619	0.115	0.203	0.231	-0.301
Mn	0.796	0.052	0.001	-0.017	0.852	0.258
Pb	0.927	-0.129	0.902	-0.203	-0.232	0.029
Zn	0.752	0.742	-0.413	-0.061	0.080	0.146
Se	0.804	0.224	0.015	-0.867	0.020	0.039
Fe	0.636	0.205	-0.278	-0.223	0.631	-0.263
Al	0.843	0.894	0.164	0.045	0.050	0.113
Cd	0.570	0.648	-0.128	-0.352	-0.042	0.093
Cr	0.481	0.192	-0.152	0.537	-0.362	0.040
Ba	0.713	-0.804	-0.155	0.081	0.170	-0.076
Percentage of Variance Explained		26.012	19.074	9.964	9.270	8.551
Total Variance Explained		72.87%				
Eigen Value		Greater than 1				

Blue cells: positive factor loading; grey cells: negative factor loading

Geochemical mechanisms of suspended solid (SS)

Southwest monsoon (SWM) Factor 1 has strong positive loading (> 0.5) of Cu, Mn, and Zn along with saline water-induced parameters like salinity, turbidity, and SS along with negative loading of pH, DO, Al, and Se. This component shows the highest positive factor score near the river mouth and the lowest in the upper part (Fig. 7a). The negative loading of Al and Se along with pH and DO indicate the absorption of Se by Al-oxyhydroxides under high pH and high DO conditions due to their reactive surfaces (Hsu 1989; Jiann and Ho 2014; Hao et al. 2020). The low negative factor scores at stations 20 and 40 km confirm such absorption in the upper part of the estuary (Fig. 7a). On the other end, the positive loading of Cu, Mn, and Zn indicates towards the release of these metals from pore water mainly due to density stratification as a result of high salinity gradient, which causes organic respiration and maintains an acidic environment near the sediment–water interface (Turner and Millward 2000). This condition is confirmed by the

negative loading of both pH and DO in this factor. These released metals are being absorbed with the help of Mn-oxyhydroxides formation on the ambient and diluent SS while replacing Fe and Al-hydroxides formed in the upstream section. In the presence of organic acids generated from their respiration, Mn hydroxides have more reactive properties than Al hydroxides (Qin et al. 2018; Habibah et al. 2014), which might be the reason behind such absorption. With this effect, Al and Fe are removed from the water column by the aggregation and precipitation of diaspore in distinct flocculation zones because of increasing ionic strength, as the water is subjected to steep pH and salinity gradients (Ferguson and Eyre 1999), whereas Se goes to dissolved phase with such effect and selecting an increase in water during SWM. This process is dominant in the lower part of the estuary (Fig. 7c). Factor 2 has major loading of Se, Fe, and Ba; meanwhile, there is a significant negative loading of Al, Mn, and Zn. The positive association of Fe, Se, and Ba indicates the absorption of these metals by Fe-oxyhydroxides (Zhang et al. 2014), and a high positive factor score is observed at
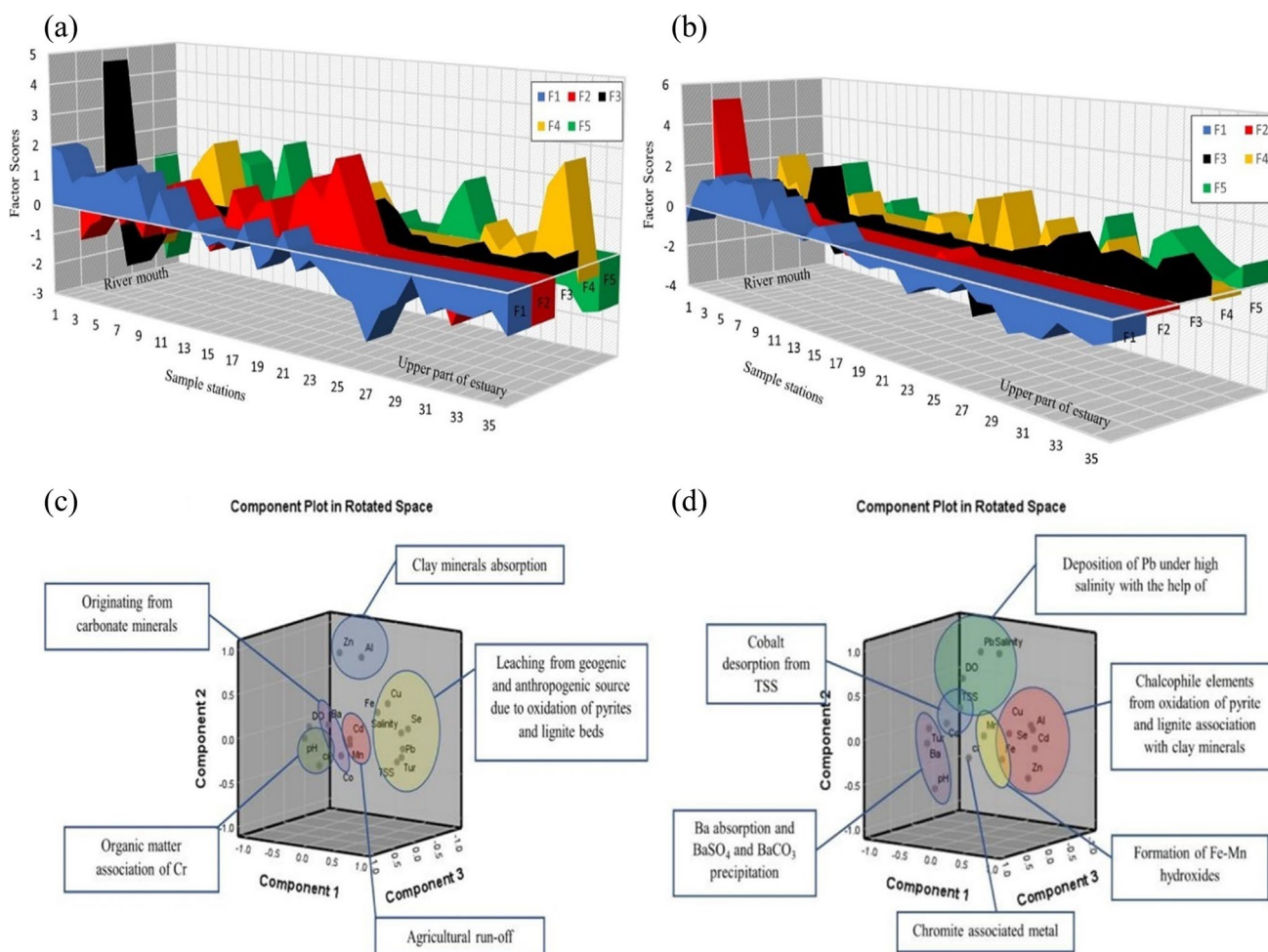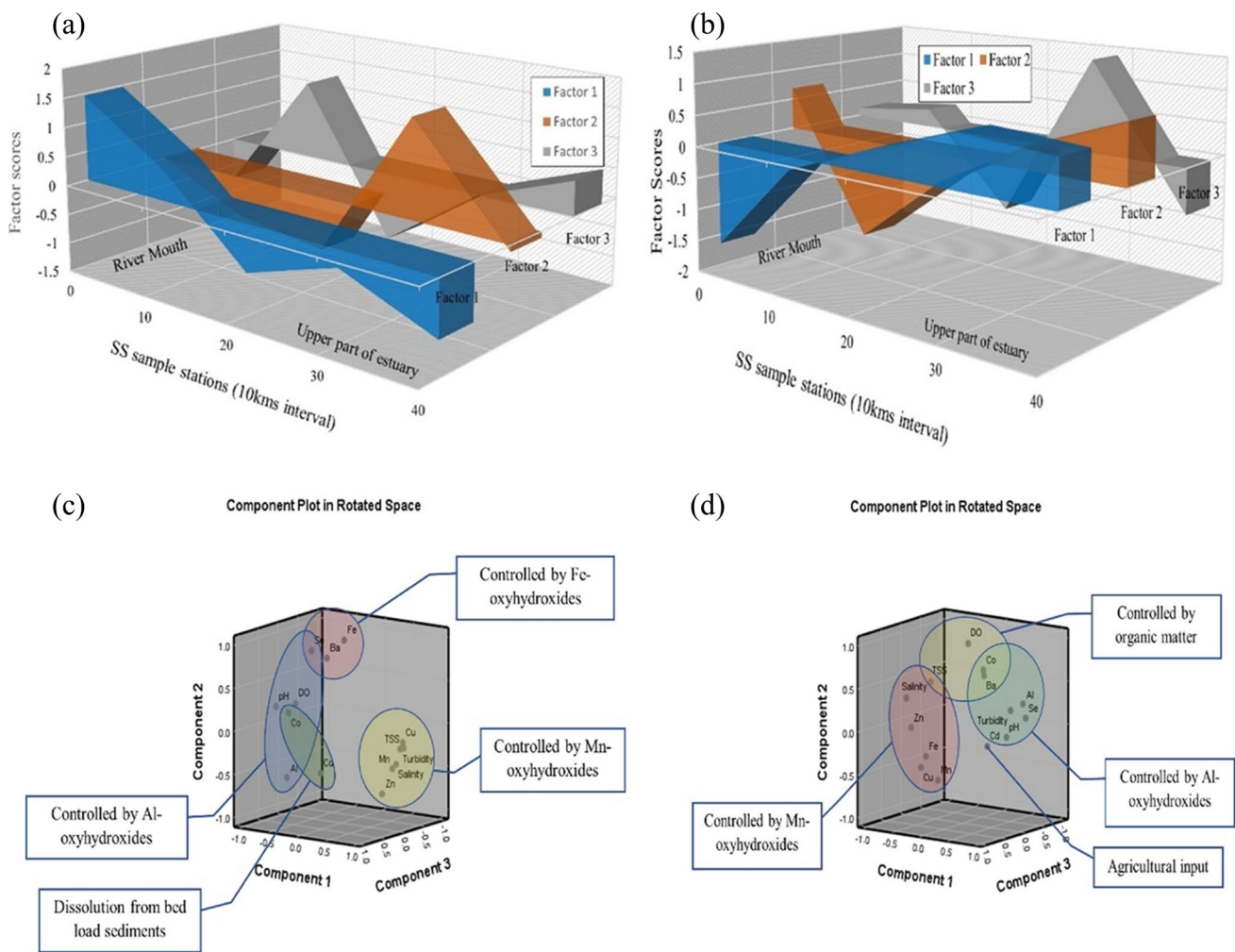
Fig. 6 Graphical representation of factors scores (**a** SWM; **b** NEM) and dominating principal components (**c** SWM; **d** NEM) for sediments

the 30-km station (Fig. 7a). As Fe is the dominating trace metal in the SS, the particulate Fe might indicate the presence of Fe $(OH)_3$ and Fe $(OH)_4^-$ (Ferguson and Eyre 1999). The tendency of Ba (Mori et al. 2019) and Se (Hung and Shy 1995; Kieliszek 2019) to form oxides with Fe in better-oxygenated conditions far away from the sea is giving rise to the increase in the concentration of these metals in the estuary, which eventually decreases towards the river mouth. The negative loading of Al, Zn, and Mn has been in the intermediate zone of the estuary, which is confirmed by the peak negative factor score from the station at 20th to 30th km (Fig. 7a). This part is the mixing zone with the partial influence of freshwater and saltwater, and such association suggests the absorption of Zn by both ambient Mn-oxyhydroxides and diluent Al-oxyhydroxides. It works as a buffer zone for both oxyhydroxides as the river mouth is dominated by Mn-oxyhydroxides due to organic respiration and acidic condition additionally by significant influence of saltwater-induced turbidity, while the upper part is mainly dominated by Al-oxyhydroxides as discussed earlier, due to ambient

DO and higher pH in factor 1. Factor 3 shows positive loading of Co and Cd along with negative loading of Mn. The high positive factor score is observed at a 10-km distance from the river mouth (Fig. 7a). This station is also associated with a major spike in the concentrations of Co and Cd during this season. As discussed before, the decisive factor behind the control of Co into the water column is bedload sediments rather than suspended particulate matter in the estuary. The majority of Co occurs mainly in a non-reactive form and is buried with accumulating sediments (Gendron et al. 1986). In the case of Cd, particulate Cd tends to settle at the sediment surface that is mostly bound to biogenic material present on it (Boyle et al. 1976; Gendron et al. 1986). But both these metals follow a redox-sensitive pattern of dissolution in the reducing zone of the sediments leading to vertical migration into the water column and enrichment by precipitation in the oxidized surface layer. In addition, these metals have an affinity towards Mn-hydroxides during redistribution in particulate form (Gendron et al. 1986). The formation of particulate Mn hydroxides in reducing zones
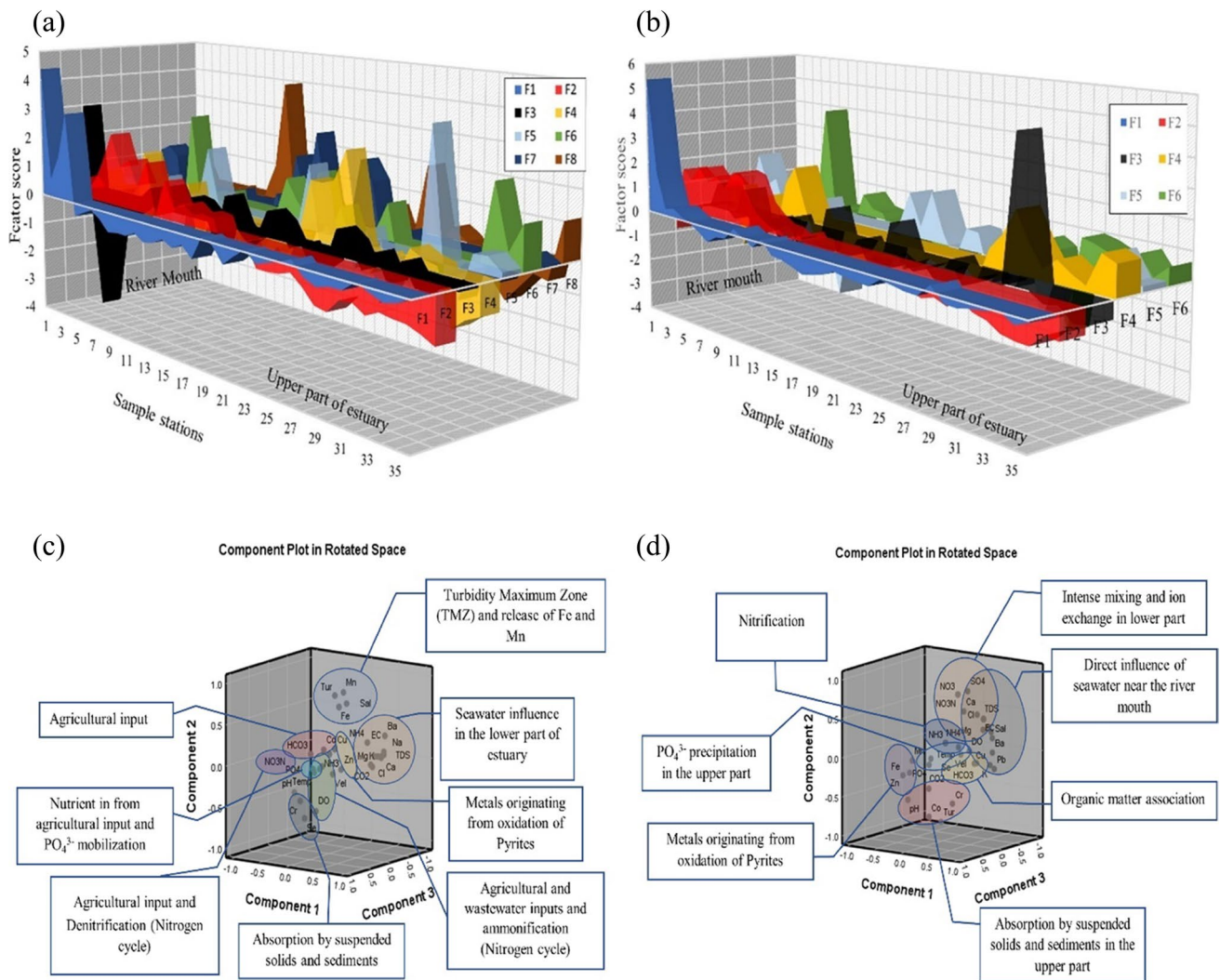
Fig. 7 Graphical representation of factors scores (**a** SWM; **b** NEM) and dominating principal components (**c** SWM; **d** NEM) for suspended solids

is evident from the earlier discussion to unravel the process governing factor 1. The association of Co and Cd from bed sediments and Mn hydroxide presence as particulate matter might be responsible for the negative loading of Mn. The released dissolved Co and Cd are being absorbed by the Mn hydroxides in the water table (Fig. 7c), which explains this association and the spike in concentration observed at station 2 (10 km) (Fig. 7a).

Northeast monsoon (NEM) Factor 1 has a strong loading of Co, Se, Al, Ba, turbidity, and pH along with negative loading of salinity, Cu, Mn, and Zn, which explains 51.49% of the total variance (Fig. 6d). This factor is very similar to the process observed in factor-1 during SWM. The association of Al, Se, Ba, and Co indicates absorption by Al oxyhydroxides under ideal pH (4–7) levels in the upper region of the estuary. In this pH range, Al-oxyhydroxides stay in insoluble particulate form (Ferguson and Eyre 1999) and

absorb metals like Co, Se and Ba due to high surface reactivity (Hsu 1989; Jiann and Ho 2014; Qin et al. 2018; Mori et al. 2019; Hao et al. 2020). But the influential region for this process in factor-1 (NEM) is higher compared to SWM. The factor scores indicate the domination of positive factor in the upper part (20 to 40 km) due to dominance of freshwater and gradually decreasing towards the station at 10 km with a gradual increase in salinity (Fig. 6b). Starting from this point, negative factor score is observed to be dominating the lower part, with the higher loading of Mn, Zn, and Cu (Fig. 6b). This part of the estuary is controlled by reducing conditions due to stratification of salt and freshwater, and the pH drops due to respiration of organic matter, which are responsible for the injection of dissolved Mn, Cu, and Zn from pore water into the water column (Turner and Millward 2000). This leads to the formation of Mn-oxyhydroxides and the absorption of metals like Cu and Zn,

Fig. 8 Graphical representation of factors scores (**a** SWM; **b** NEM) and dominating principal components (**c** SWM; **d** NEM) for water

which was also observed during NEM (factor 1). Factor 2 has significant loading of Co, Ba, DO, and TSS along with negative loading of Cu and Mn, which explains 26.02% of the variance (Fig. 6d). This indicates the common origin of these metals and is mainly obtained from the oxidation of pyrite concretion in the source rocks and weathering of shale. All the metals obtained in this factor is reported to be available in the concretion. The DO in such a process works as an oxidant and the process is likely to take place in well-oxygenated conditions (Moses et al. 1987). The association of TSS with these metals in the absence of any controlling oxides or clay minerals indicates the absorption of Co and Ba by particulate organic matter, which are highly reactive in prevailing conditions. The higher positive factor score in the upper part supports this theory as the upper part of the estuary is observed to be dominated by freshwater (Fig. 6d). On the other hand, both Cu and Mn show a spike in trend in the lower part, and an especially significant negative

factor score is obtained at station SS2 (10 km from the river mouth) (Fig. 6d). This station falls under the high mixing zone in this season and higher seawater influence leading to respiration of the mentioned organic matter, thus leading to the dissolution of Co and Ba, while making Mn oxyhydroxides more reactive with a generated organic acid in the process (Qin et al. 2018; Habibah et al. 2014) which leads to the absorption of Zn. Factor 3 has significantly higher loading of TSS and Fe and negative loading of Cd indicating the different origins of the metals, where most of the Fe concentration is geogenic and Cd concentration acquired from the SS is from anthropogenic sources like agricultural inputs. The association of TSS and Fe indicates the presence of particulate Fe in the water table, and both metals are associated with run-off water carrying SS from the river basin and agricultural fields (Pobi et al. 2019). This factor explains 16.11% of the total variance.

Geochemical mechanisms of sediment (< 63-μm fraction)

Southwest monsoon (SWM) Factor 1 represents 27.02% of the total variance and is explained by the significant positive loadings of Pb, Se, Fe, salinity, TSS, and turbidity and a significant negative loading of DO. These elements are mainly associated with Fe-oxy-hydroxides, and their concentrations are influenced by the salinity. This indicates absorption and settlement of Se containing Fe-oxyhydroxides due to increasing seawater influence near the mouth (Fig. 6a) where Mn-oxyhydroxides dominate the absorption process as suspended solids. Such absorption was observed in the water column by SS in both water (factor-2-tidal influenced turbidity region) (Fig. 6a) and SS (Fig. 7a: upper part) factor models aforementioned. Of the positive loadings of Fe, Pb and Se in factor 1 indicates that these metals are leached from geogenic sources like pyrites and lignite beds present in the Sibuti Formation (Nagarajan et al. 2017a) and peat soil exposed within the river basin area as these elements are rich in Fe, Pb, Cu (Sia and Abdullah 2012), and Se (Yudovich and Ketris 2006; Chang et al. 2020) (Fig. 6c). Factor 2 has significant loading of Al and Zn with a variance of 12.41% in the intermediate zones during SWM (Fig. 6c). This suggests absorption of Zn on clay minerals and Al-oxyhydroxides in the intermediate zone of the estuary. Such condition was noticed in the intermediate zone of the estuary in the SS factor model (factor 2: Sect. 4.3.2.1) (Fig. 7c), where ambient Mn and freshwater carrying Al-oxyhydroxides (factor 2: Sect. 4.3.2.1) controlled the absorption in this zone and settlement of Al-oxyhydroxide containing metals with increasing seawater influence towards the mouth. This association indicates that these elements are mainly associated with clay minerals like illite, chlorite, and kaolinite in the estuarine sediments. Factor 3 has a high loading of pH and Cr with the explained variance of 11.64% during this season. In a pH range of 5–7, Cr (III) prevails and easily associates with reducible organic matter (Namieśnik and Rabajczyk 2010). The dominant species of Cr (III) in the pH range of 4.5 to 7.5 are Cr $(OH)^{2+}$ and Cr $(OH)_2^+$ which are susceptible to bioaccumulation through suspended solids and eventually depositing in sediments (Namieśnik and Rabajczyk 2010). Such absorption was noticed in water as aforementioned in the water factor model (factor 2: Sect. 4.3.1.1), where Fe and Mn played a major role in the absorption. This independent behaviour of Cr also stipulates towards leaching of Cr from mixed sources like pyrite and shale concretion in Sibuti Formation and siliciclastic sediments of Sibuti and Lambir formations (Nagarajan et al. 2017a) rather than chromites present in NW Borneo and Sibuti Formation in the river basin. Chromites are predominantly acid-resistant in nature and do not leach Cr under the prevailing pH condition of the estuary (Weng et al. 1994, 2001).

Factor 4 has significant loading of Co and Ba, and dissociation of these 2 elements from any other elements indicates its mixed origin like non-aluminous silicate minerals where both metals are not associated with Al oxides in the sediments of Sibuti Formation (Nagarajan et al. 2019, 2017a). In addition, carbonate (calcite, dolomite, and magnesite) or Fe oxide minerals such as goethite and pyrite might be a source as well (Dehaine et al. 2021). These minerals are abundant in shale and pyrite concretion of Sibuti and Setap formations. Factor 5 has a higher loading of Cd with high negative loading of Mn. This might be due to the variation in the origin of both metals, where Cd is a major input from agricultural fields and Mn presence is mainly from geogenic sources in the study area. Moderate loading of turbidity in this component indicates the desorption of Mn hydroxide bound Cd in high turbid conditions.

Northeast monsoon (NEM) Factor 1 has higher loading of Cu, Zn, Al, and Cd and high negative loading of Ba, turbidity, and pH. The chalcophile elements (Cu, Cd, and Zn) are derived from pyrite and shale concretion, and distribution is mainly controlled by clay minerals and phyllosilicates such as illite and kaolinite (Nagarajan et al. 2017a). The higher loading of Cd might be due to the absorption of Cd onto the clay minerals in the lower part of the estuary (Hao et al. 2020, Jiann and Ho 2014; Namiesnik and Rabajczyk 2010) (Fig. 6b). On the other hand, negative loading of Ba, turbidity, and pH indicate absorption. The association of Ba with clay minerals is well observed in arkoses in Sibuti and Lambir formations (Nagarajan et al. 2015, 2017a) which supports the association of Ba with clay minerals or Al-oxyhydroxides controlled factor in SS (factor 1: Sect. 4.3.2.2) and indicates settlement of such in the lower part of the estuary (Fig. 6d). The presence of Ba in Sibuti and Tukau Formations validates the leaching of this metal with chalcophile metals like Cu, Zn, and Cd. In addition, leached Ba in aquatic environments commonly precipitates as $BaSO_4$ or $BaCO_3$, where $BaSO_4$ is mainly associated with seawater introduction because of higher SO_4 content (Gad 2014) and respiration of organic matter, which is associated with acidic water (Marchitto 2013). The observed organic matter respiration in the water column (factor 6: Sect. 4.3.1.2) also validates the observation. Hence, formation of both precipitates are supported by absorption process in suspended solids and sedimentation with the help of Al-oxyhydroxides (Gad 2014).

Moreover, comparing the conditions during NEM, low SO_4^{2-} concentration is observed in the upper part where the upper part has high SO_4^{2-} content in the estuary and the turbidity of water has peaked in both ends while decreasing in the intermediate zone. In the case of pH, higher pH is observed in the upper part whereas relatively acidic conditions prevailed in the lower part.

Fig. 9 Average values of K_d for considered metals during SWM and NEM
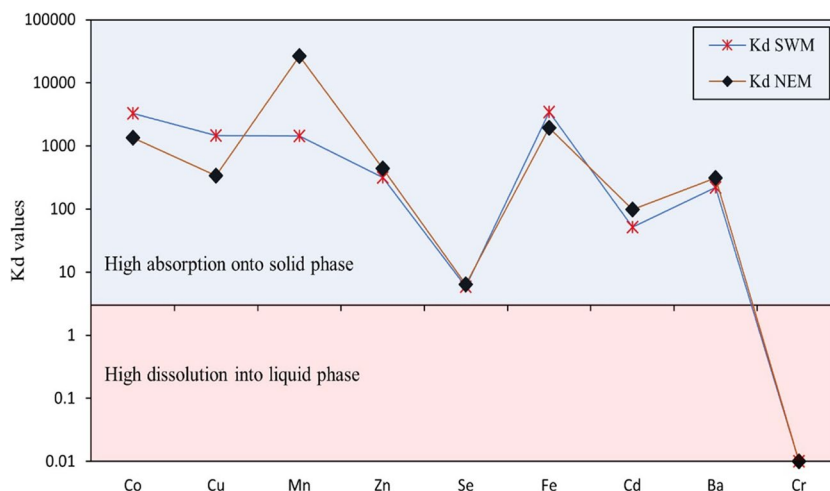
To sum up the factor with the above discussion, $BaCO_3$ precipitation is evident in the upperpart and $BaSO_4$ precipitation in the lower part under high turbidity conditions mainly controlled by absorption and sedimentation of suspended solids in the estuary. Factor 3 has high positive loading of Cr and high negative loading of Se. This kind of loading of these metals indicates the variation of origin for both metals where Cr is a ferromagnesian metal mainly derived from chromite present in the Sibuti Formation (Nagarajan et al. 2017a), while Se is a chalcophile metal mainly associated with lignite, peat soils, pyrites, and/or other heavy minerals (Yudovich and Ketris 2006) in the source region. Factor 4 has higher loading of Fe and Mn observed during NEM which might be due to the formation of Fe and Mn hydroxides and co-precipitation under well-oxygenated conditions (Fig. 6d) observed during this season (Duinker et al. 1979; Wollast et al. 1979). The higher negative loading of Co and high positive loading of TSS in factor 5, and lesser representation of metals may be attributed to the adsorption by the shale concretions in Sibuti and Lambir formations under tropical conditions (Nagarajan et al. 2017a, 2015). These oxidized metals are mainly transported in dissolved form or particulate form in river systems, where both phases pose a tendency to form metal humic complexes (Tessier et al. 1984). In addition, Co is particle reactive, and 90% of Co absorption by clay minerals is common in open river streams resembling the study area, whereas desorption up to 40–70% is observed through the introduction of seawater (Anandkumar et al. 2022). Considering these observations, this association indicates the desorption of Co from suspended solids due to prevailing hydrological conditions like the flow velocity of currents, and action by waves and tides, causing the breakdown of humic complexes with the introduction of seawater in the estuary.

Partitioning of metals between particulate and dissolved phase

The average partition coefficient values during both seasons for all the metals have been recorded to be greater than 3 (Fig. 9), except for Cr which is present in the liquid phase but absent in suspended solids. The higher value of K_d (<3) shows the affinity of metals towards SS or absorption, whereas a lower value than 3 represents a higher affinity of metals towards liquid phase or dissolution under varying environmental conditions (Kumar et al. 2010; Zheng et al. 2013; Yang and Wang 2017; Zhang et al. 2018; Sedeño-Díaz et al. 2020). This infers that the metal absorption from the liquid phase and particle reactivity of metals with SS is higher, and it is a dominating process in the estuary (Li et al. 2018). The higher mobility of trace metals during SWM and NEM can be represented as $Cr > Se > Cd > Ba > Zn > Mn > Cu > Co > Fe > Al$ and $Cr > Se > Cd > Cu > Zn > Co > Ba > Fe > Mn > Al$, respectively. The higher tendency of Mn to form hydroxides under oxidizing conditions because of freshwater dilution during NEM might facilitate increased reactivity towards SS (Duinker et al. 1979; Wollast et al. 1979; Oldham et al. 2017; Mori et al. 2019). On the other hand, the behaviour of Al and Cr remains the same as SWM, since the oxidizing conditions favor the formation of readily soluble Cr (VI) in water and the insoluble nature of Al under prevailing pH conditions prevents it from being mobile (Namieśnik and Rabajczyk 2010). The K_d shown by Zn, Se, Fe, and Cd is almost constant during both seasons (Fig. 9), whereas lower absorption of Co and Cu has been noticed during NEM.

Isotopic signatures in estuarine water

The descriptive statistical composition of δD, $δ^{18}O$, and d-excess is presented in Table 1. The composition of estuarine water samples collected during SWM and NEM shows the value of δD, ranging from -85.41 to $-72.55‰$

Fig. 10 δD versus δ^{18}O of Sibuti estuarine samples of SWM and NEM compared with LWML and GMWL
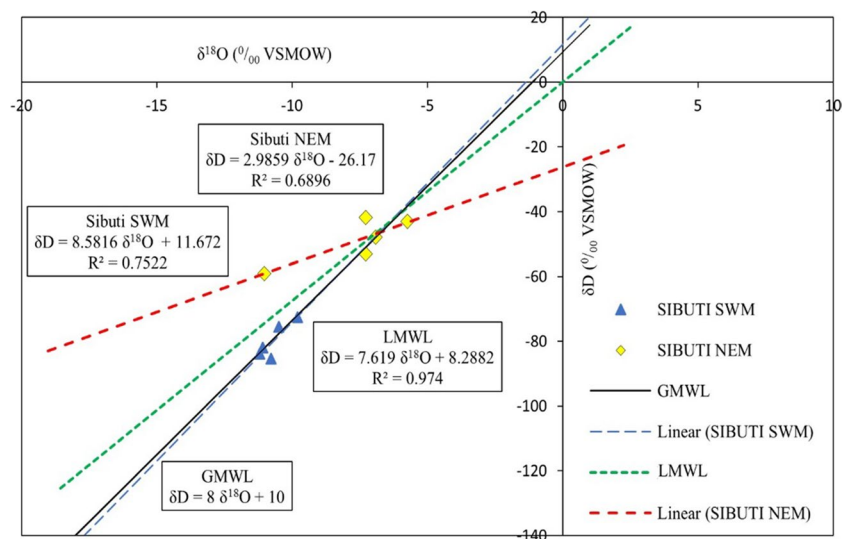
and −59.06 to −41.89‰ with respective mean values of −79.88 and −48.99‰. Similarly, δ^{18}O in estuary deviated from −11.20 to −9.80‰ during SWM and −11.02 to −5.74‰ during NEM with mean values of −10.67 and −7.64‰, respectively. The value of d-excess ranged from 0.83 to 8.25‰ with a mean value of 5.47‰ during SWM, whereas it ranged from 2.89 to 29.10‰ with a mean value of 12.15‰ during NEM.

X–Y scatter plot was considered with fitted regression line for δ^{18}O, δD, and LWML derived from Limbang area (Valappil et al. 2022), which is close to the study area (Fig. 10). The samples during SWM were plotted close to GMWL and LMWL (Fig. 10) indicating that meteoritic water was the main source of the water in the estuary, whereas NEM samples were significantly deviated from LMWL and GMWL clearly indicating an evaporation trend. However, both the regression lines intersect LWML and GMWL at an approximate common point indicating a particular location might be the source of the precipitation during both seasons (Ongetta et al. 2022). The intersection suggests that precipitation near Limbang city, Sarawak, is the main source of water in the estuary. The relationship with LMWL is determined using equations obtained in Fig. 10. The samples of SWM have a slope of 8.58 with a *d*-intercept of 11.67, whereas NEM has a slope of 2.98 with a *d*-intercept of −26.17. This significant difference in slope indicates different moisture sources during both seasons (Datta et al. 1991). The higher slope and *d*-intercept during SWM strengthen the influence of raindrop re-evaporation (Anati and Gat 1989; Liu et al. 2014). On the other hand, a lesser slope and high negative *d*-intercept during NEM indicate intense evaporation (Liu et al. 2014).

Assessment of d-excess is useful to determine the contribution of moisture source (Gat and Carmi 1970; Deshpande et al. 2013a, b; Thivya et al. 2016; Valappil et al. 2022). Significant variable average d-excess values recorded during

SWM and NEM suggest the involvement of additional processes apart from condensation from ocean evaporation or primary precipitation during the generation of moisture (Dansgaard 1964; Valappil et al. 2022; Sabarathinam et al. 2020). SWM has d-excess < 10‰, which might attribute to the secondary evaporation of raindrops due to high humidity in the source region (Clark and Fritz 1997; Gautam et al. 2017; Benetti et al. 2014). On the other hand, NEM has an average *d*-excess > 10‰, which might be due to the evaporative effect from recycled terrestrial moisture such as rivers, sea, and lakes under low humidity conditions (Chidambaram et al. 2009; Valappil et al. 2022) or a mixture of various terrestrial run-off (Deshpande et al. 2013a, b).

Conclusion

In this study, the spatial distribution, geochemistry, and potential sources of various elements during SWM and NWM were investigated for the Sibuti River estuary and the following implications were derived:

- δD and δ^{18}O values revealed that precipitation over northern Sarawak was the main source of precipitation. Though Raindrop evaporation was evident during SWM, whereas intense evaporation was noticed in NEM samples. Evaporative effluents from recycled terrestrial moisture and their re-evaporation were found to be the controlling sources for the moisture.

- Seawater dominance is consistent in the estuary irrespective of the monsoons, where Na-Cl water type is dominant during low flow, whereas mixed type Ca–Mg–Cl coupled with reverse ion exchange dominated the estuary during high flow. Similarly, tidal resistance generated by the SCS works as a key component for the

dissolution of minerals where low flow is associated with increased degassing of CO_2 due to higher residence time of water causing higher dissolution of halite and carbonates, whereas high flow with high discharge of river has a control over sulfate dissolution. The prevailing dominance of tidal water and existing hydrodynamic gradient makes the estuary more absorptive in nature by resuspension and deposition of bed load sediments as suspended solids under ideal pH conditions (4–7).

- Statistical evaluation reconfirmed the dominating tidal influence in the estuary that plays a major role in regulating the major ions (Cl^-, Mg^{2+}, Ca^{2+}, Na^+, K^+, HCO_3^-, and SO_4^{2-}) irrespective of the seasons. The nitrogen cycle is evident in the estuary, where nitrification, denitrification, and ammonification are major processes during both seasons in the lower and intermediate zones of the estuary. In addition, the oxidation of organic matter was dominant in the turbidity maximum zone (TMZ) due to anaerobic conditions prevailing near the river mouth giving rise to organic-induced negatively charged Mn-oxyhydroxide collides, control the absorption in the lower reaches during both seasons facilitating Cd and Zn concentrations in suspended solids. The absorption in the intermediate zone and upper reaches are controlled by Al-oxyhydroxides and Fe-oxyhydroxides, and their settlement in the lower reaches due to increased seawater influence makes them dominant in the sediments and thus serve as major carriers of metals such as Co, Cr, Ba, Se, Cu, and Pb.

- Nutrients such as NO_3^-, NH_3, NH_4^+, and PO_4^{3-} were originated from agricultural activities in the river basin whereas wastewater effluents from Bekenu were found to be the major contributor of NH_3. The trace metals mainly originated from geogenic sources, especially from shale and pyrite concretion of the Sibuti Formation and siliciclastic sediments of the Sibuti and Lambir formations. The study also infers that oxidation and high deforestation coupled with a high degree of chemical weathering due to higher rainfall might be the major contributor for the higher concentrations of trace metals in the river and estuary.

Declarations

References

Anandkumar A, Nagarajan R, Eswaramoorthi S, Prabakaran K (2022) Seasonal variation and mobility of trace metal in the beach sediments of NW Borneo. Chemosphere 287:132069. https://doi.org/10.1016/j.chemosphere.2021.132069

Anati DA, Gat JR (1989) Restricted marine basins and marginal sea environments. In: Fritz P, Fontes JC (eds) Handbook of environmental isotope geochemistry, vol 3. Elsevier, Amsterdam, pp 29–73

Annapoorna H, Janardhana MR (2015) Assessment of groundwater quality for drinking purpose in rural areas surrounding a defunct copper mine. Aquatic Procedia 4:685–692

APHA (1998) Standard methods for the examination of water and wastewater, 19th edn. USASS, APHA, Washington, DC

Asha AS, Saifullah ASM, Uddin MG, Sheikh MS, Uddin MJ, Diganta MTM (2020) Assessment of trace metal in macroalgae and sediment of the Sundarban mangrove estuary. Appl Water Sci 10(1):1–13

Azrul NIsyam BK, Ching Siu J, Joelle Lee MS, Lucian Ng FL, Mohammad Amir Syafiz BMN, Muhammad Syafiz BR, Woon Z (2013) Geochemistry of concretions in sedimentary rocks of Setap Shale, Northwest Borneo, Malaysia. BSC dissertation submitted to Curtin Unviersity, Malaysia (unpublished)

Baric A, Kuspilic G, Matijevic S (2002) Nutrient (N, P, Si) fluxes between marine sediments and water column in coastal and open Adriatic. Hydrobiologia 475(1):151–159

Benetti M, Reverdin G, Pierre C, Merlivat L, Risi C, Steen-Larsen HC, Vimeux F (2014) Deuterium excess in marine water vapor: dependency on relative humidity and surface wind speed during evaporation. J Geophys Res: Atmos 119(2):584–593

Bewers JM, Yeats PA (1978) Trace metals in the waters of a partially mixed estuary. Estuar Coast Mar Sci 7(2):147–162

Boomer KMB, Bedford BL (2008) Influence of nested groundwater systems on reduction–oxidation and alkalinity gradients with implications for plant nutrient availability in four New York fens. J Hydrol 351(1–2):107–125

Boothroyd JC (1978) Mesotidal inlets and estuaries. In: Davis RA (ed) Coastal sedimentary environments. Springer, New York, NY, pp 287–360. https://doi.org/10.1007/978-1-4684-0056-4_7

Boyle EA, Sclater F, Edmond JM (1976) On the marine geochemistry of cadmium. Nature 263(5572):42–44

Boyle EA, Edmond JM, Sholkovitz ER (1977) The mechanism of iron removal in estuaries. Geochim Cosmochim Acta 41(9):1313–1324

Brantley SL, Lebedeva MI, Balashov VN, Singha K, Sullivan PL, Stinchcomb G (2017) Toward a conceptual model relating chemical reaction fronts to water flow paths in hills. Geomorphology 277:100–117

Browne N, Braoun C, McIlwain J, Nagarajan R, Zinke J (2019) Borneo coral reefs subject to high sediment loads show evidence of resilience to various environmental stressors. PeerJ 7:e7382

Callaway RJ, Specht DT, Ditsworth GR (1988) Manganese and suspended matter in the Yaquina estuary. Oregon Estuaries 11(4):217–225

Campbell JA, Yeats PA (1984) Dissolved chromium in the St. Lawrence estuary. Estuarine Coastal Shelf Sci 19(5):513–522

Canfield DE, Thamdrup B, Hansen JW (1993) The anaerobic degradation of organic matter in Danish coastal sediments: iron reduction, manganese reduction, and sulfate reduction. Geochim Cosmochim Acta 57(16):3867–3883

Chang Y, Müller M, Wu Y, Jiang S, Cao WW, Qu JG, ..., Mujahid A (2020) Distribution and behaviour of dissolved selenium in tropical peatland-draining rivers and estuaries of Malaysia. Biogeosciences 17(4):1133–1145

Chidambaram S, PrasannaMV Ramanathan AL, Vasu K, Hameed S, Warrier UK, Srinivasamoorthy K, Manivannan R, Tirumalesh K, Anandhan P, Johnsonbabu G (2009) A study on the factors affecting the stable isotopic composition in precipitation of Tamil Nadu, India. Hydrol Process 23(12):1792–1800. https://doi.org/10.1002/hyp.7300

Chidambaram S, Prasanna MV, Karmegam U, Singaraja C, Pethaperumal S, Manivannan R, ..., Tirumalesh K (2011) Significance of pCO_2 values in determining carbonate chemistry in groundwater of Pondicherry region, India. Front Earth Sci 5(2):197

Chopard A, Plante B, Benzaazoua M, Bouzahzah H, Marion P (2017) Geochemical investigation of the galvanic effects during oxidation of pyrite and base-metals sulfides. Chemosphere 166:281–291

Clark I, Fritz P (1997) Environmental Isotopes in Hydrogeology. CRC Press, New York, p 342

Cochran JK (2014) Estuaries, module in earth systems and environmental sciences, Elsevier, ISBN 9780124095489. https://doi.org/10.1016/B978-0-12-409548-9.09151-X

Coffey M, Dehairs F, Collette O, Luther G, Church T, Jickells T (1997) The behaviour of dissolved barium in estuaries. Estuar Coast Shelf Sci 45(1):113–121

Craig H (1961) Isotopic variations in meteoric waters. Science 133(3465):1702–1703

Dansgaard W (1964) Stable isotopes in precipitation. Tellus 16(4):436–468

Datta PS, Tyagi SK, Chandrasekharan H (1991) Factors controlling stable isotope composition of rainfall in New Delhi India. J Hydrol 128(1–4):223–236

De Boo W (1990) Cadmium in agriculture. Toxicol Environ Chem 27(1–3):55–63

Deborde J, Anschutz P, Chaillou G, Etcheber H, Commarieu MV, Lecroart P, Abril G (2007) The dynamics of phosphorus in turbid estuarine systems: example of the Gironde estuary (France). Limnol Oceanogr 52(2):862–872

Dehaine Q, Tijsseling LT, Glass HJ, Törmänen T, Butcher AR (2021) Geometallurgy of cobalt ores: a review. Miner Eng 160:106656

Deshpande RD, Maurya AS, Angasaria RC, Dave M, Shukla AD, Bhandari N, Gupta SK (2013a) Isotopic studies of megacryometeors in western India. Curr Sci 104(6):728–737

Deshpande RD, Muraleedharan PM, Singh RL, Kumar B, Rao MS, Dave M, ..., Gupta SK (2013b) Spatio-temporal distributions of δ18O, δD and salinity in the Arabian Sea: identifying processes and controls. Marine Chemistry, 157, 144–161.

Drogowska M, Brossard L, Ménard H (1994) Comparative study of copper behaviour in bicarbonate and phosphate aqueous solutions and effect of chloride ions. J Appl Electrochem 24(4):344–349

Duinker JC, Wollast R, Billen G (1979) Behaviour of manganese in the Rhine and Scheldt estuaries: II. Geochemical cycling. Estuarine Coastal Mar Sci 9(6):727–738

Eisma D (1988) Transport and deposition of suspended matter in estuaries and the Nearshore Sea. In: Lerman A, Meybeck M (eds) Physical and chemical weathering in geochemical cycles. NATO ASI series, vol 251. Springer, Dordrecht, pp 273–298

Ferguson A, Eyre B (1999) Behaviour of aluminium and iron in acid runoff from acid sulphate soils in the lower Richmond River catchment. J Aust Geol Geophys 17(5/6):193–202

Fernandez A, Borrok DM (2009) Fractionation of Cu, Fe, and Zn isotopes during the oxidative weathering of sulfide-rich rocks. Chem Geol 264(1–4):1–12

Ferrer MR, Quevedo-Sarmiento J, Rivadeneyra MA, Bejar V, Delgado R, Ramos-Cormenzana A (1988) Calcium carbonate precipitation by two groups of moderately halophilic microorganisms at different temperatures and salt concentrations. Curr Microbiol 17:221–227

Frazar S, Gold AJ, Addy K, Moatar F, Birgand F, Schroth AW, ..., Pradhanang SM (2019) Contrasting behavior of nitrate and phosphate flux from high flow events on small agricultural and urban watersheds. Biogeochemistry, 145(1), 141–160.

Gad SC (2014) Barium. In: Philip Wexler (ed) Encyclopedia of toxicology, 3rd edn. Academic Press, pp 368–370. ISBN 9780123864550. https://doi.org/10.1016/B978-0-12-386454-3.00819-8

Galán E, Gómez-Ariza JL, González I, Fernández-Caliani JC, Morales E, Giráldez I (2003) Heavy metal partitioning in river sediments severely polluted by acid mine drainage in the Iberian Pyrite Belt. Appl Geochem 18(3):409–421

Gandaseca S, Rosli N, Ngayop J, Arianto CI (2011) Status of water quality based on the physico-chemical assessment on river water at Wildlife Sanctuary Sibuti Mangrove Forest, Miri Sarawak. Am J Environ Sci 7(3):269

Gat JR, Carmi I (1970) Evolution of the isotopic composition of atmospheric waters in the Mediterranean Sea area. J Geophys Res 75(15):3039–3048

Gautam MK, Lee KS, Bong YS, Song BY, Ryu JS (2017) Oxygen and hydrogen isotopic characterization of rainfall and throughfall in four South Korean cool temperate forests. Hydrol Sci J 62(12):2025–2034

Geisler E, Bogler A, Bar-Zeev E, Rahav E (2020) Heterotrophic nitrogen fixation at the hyper-eutrophic Qishon river and estuary system. Front Microbiol 11:1370

Gendron A, Silverberg N, Sundby B, Lebel J (1986) Early diagenesis of cadmium and cobalt in sediments of the Laurentian Trough. Geochim Cosmochim Acta 50(5):741–747

Gibbs RJ (1970) Mechanisms controlling world water chemistry. Science 170(3962):1088–1090

Gibbs RJ (1973) Mechanisms of trace metal transport in rivers. Science 180(4081):71–73

Greger M, Kautsky L, Sandberg T (1995) A tentative model of Cd uptake in Potamogeton pectinatus in relation to salinity. Environ Exp Bot 35(2):215–225

Guinoiseau D, Bouchez J, Gélabert A, Louvat P, Filizola N, Benedetti MF (2016) The geochemical filter of large river confluences. Chem Geol 441:191–203

Haaijer SC, Van der Welle ME, Schmid MC, Lamers LP, Jetten MS, Op den Camp HJ (2006) Evidence for the involvement of betaproteobacterial Thiobacilli in the nitrate-dependent oxidation of iron sulfide minerals. FEMS Microbiol Ecol 58(3):439–448

Habibah J, Khairiah J, Ismail BS, Kadderi MD (2014) Manganese speciation in selected agricultural soils of peninsular Malaysia. Am J Environ Sci 10(2):148

Hamzaoui-Azaza F, Tlili-Zrelli B, Bouhlila R, Gueddari M (2013) An integrated statistical methods and modelling mineral–water interaction to identifying hydrogeochemical processes in groundwater in Southern Tunisia. Chem Speciat Bioavailab 25(3):165–178

Hao W, Kashiwabara T, Jin R, Takahashi Y, Gingras M, Alessi DS, Konhauser KO (2020) Clay minerals as a source of cadmium to estuaries. Sci Rep 10:10417

Hartzell JL, Jordan TE (2012) Shifts in the relative availability of phosphorus and nitrogen along estuarine salinity gradients. Biogeochemistry 107(1–3):489–500

Hirst C, Andersson PS, Shaw S, Burke IT, Kutscher L, Murphy MJ, ..., Porcelli D (2017) Characterisation of Fe-bearing particles and colloids in the Lena River basin, NE Russia. Geochimica et Cosmochimica Acta 213:553–573

Hsu PH (1989) Aluminum hydroxides and oxyhydroxides. Min Soil Environ 1:331–378

Huang Z, Liu C, Zhao X, Dong J, Zheng B (2020) Risk assessment of heavy metals in the surface sediment at the drinking water source of the Xiangjiang River in South China. Environ Sci Eur 32(1):1–9

Hung JJ, Shy CP (1995) Speciation of dissolved Selenium in the Kaoping and Erhjen Rivers and Estuaries, southwestern Taiwan. Estuaries 18(1):234–240

Hutchison CS (1996) The 'Rajang accretionary prism' and 'Lupar Line' problem of Borneo. Geol Soc London Spec Publ 106(1):247–261

Hutchison CS (2005) Geology of North-West Borneo: Sarawak. Elsevier, Brunei and Sabah

Iglesias I, Almeida CMR, Teixeira C, Mucha AP, Magalhães A, Bio A, Bastos L (2020) Linking contaminant distribution to hydrodynamic patterns in an urban estuary: the Douro estuary test case. Sci Total Environ 707:135792

Ishak AK, Samuding K, Yusoff NH (2001) Water and suspended sediment dynamics in Selangor River estuary. Proceedings of the Malaysian science and technology congress 2000: symposium A, vol II. Malaysia: confederation of scientific and technological associations in malaysia COSTAM, p 415

Jezierska B, Ługowska K, Witeska M (2009) The effects of heavy metals on embryonic development of fish (a review). Fish Physiol Biochem 35(4):625–640

Jiann KT, Ho P (2014) Cadmium mixing behavior in estuaries: redox controls on removal and mobilization. TAO: Terr Atmos Ocean Sci 25(5):655

Jilbert T, Tiihonen R, Myllykangas JP, Asmala E, Hietanen S (2016) Reactive iron and manganese in estuarine sediments of the Baltic Sea: impacts of flocculation and redox shuttling. EGU General Assembly 2016, Vienna Austria, id. EPSC2016–14808

Juen LL, Aris AZ, Shan NT, Yusoff FM, Hashim Z (2015) Geochemical modeling of element species in selected tropical estuaries and coastal water of the Strait of Malacca. Procedia Environ Sci 30:109–114

Karbassi AR, Tajziehchi S, Adib NF (2016) Role of estuarine natural processes in removal of trace metals under emergency situations. Glob J Environ Sci Manag 2(1):31

Kieliszek M (2019) Selenium–fascinating microelement, properties and sources in food. Molecules 24(7):1298

Klimchouk A, Cucchi F, Calaforra JM, Aksem S, Finocchiaro F, Forti P (1996) Dissolution of gypsum from field observations. Int J Speleol 25(3):3

Koukina SE, Lobus NV, Shatravin AV (2021) Multi-element signatures in solid and solution phases in a tropical mixing zone: a case study in the Cai River estuary Vietnam. Chemosphere 280:130951

Krawczyk H, Zinke J, Browne N, Struck U, McIlwain J, O'Leary M, Garbe-Schönberg D (2020) Corals reveal ENSO-driven synchrony of climate impacts on both terrestrial and marine ecosystems in northern Borneo. Sci Rep 10(1):1–14

Kronvang B, Laubel A, Larsen SE, Friberg N (2003) Pesticides and heavy metals in Danish streambed sediment. Hydrobiologia 494(1–3):93–101

Kumar B, Senthil Kumar K, Priya M, Mukhopadhyay D, Shah R (2010) Distribution, partitioning, bioaccumulation of trace elements in water, sediment and fish from sewage fed fishponds in eastern Kolkata, India. Toxicol Environ Chem 92(2):243–260

Lamers LP, Falla SJ, Samborska EM, Dulken IAV, Hengstum GV, Roelofs JG (2002) Factors controlling the extent of eutrophication and toxicity in sulfate-polluted freshwater wetlands. Limnol Oceanogr 47(2):585–593

Ledesma-Ruiz R, Pastén-Zapata E, Parra R, Harter T, Mahlknecht J (2015) Investigation of the geochemical evolution of groundwater under agricultural land: a case study in northeastern Mexico. J Hydrol 521:410–423

Li R, Tang C, Cao Y, Jiang T, Chen J (2018) The distribution and partitioning of trace metals (Pb, Cd, Cu, and Zn) and metalloid (As) in the Beijiang River. Environ Monit Assess 190(7):399

Lintern A, Webb JA, Ryu D, Liu S, Bende-Michl U, Waters D, Leahy P, Wilson P, Western AW (2018) Key factors influencing differences in stream water quality across space. Wiley Interdiscip Rev Water 5(1):e1260

Liu J, Xiao C, Ding M, Ren J (2014) Variations in stable hydrogen and oxygen isotopes in atmospheric water vapor in the marine boundary layer across a wide latitude range. J Environ Sci 26(11):2266–2276

Lu L, Wang R, Chen F, Xue J, Zhang P, Lu J (2005) Element mobility during pyrite weathering: implications for acid and heavy metal pollution at mining-impacted sites. Environ Geol 49(1):82–89

Lučić M, Jurina I, Ščančar J, Mikac N, Vdović N (2019) Sedimentological and geochemical characterization of river suspended particulate matter (SPM) sampled by time-integrated mass flux sampler (TIMS) in the Sava River (Croatia). J Soils Sediments 19:989–1004

Malcolm SJ, Battersby NS, Stanley SO, Brown CM (1986) Organic degradation, sulphate reduction and ammonia production in the sediments of Loch Eil, Scotland. Estuar Coast Shelf Sci 23(5):689–704

MANRED, (Ministry of Modernisation of Agriculture, Native Land and Regional Development Sarawak) (2020) Retrieved from

https://manred.sarawak.gov.my/modules/web/pages.php?mod=news&sub=news_view&nid=338. Accessed Dec 2020

Mapoma HWT, Xie X, Liu Y, Zhu Y, Kawaye FP, Kayira TM (2017) Hydrochemistry and quality of groundwater in alluvial aquifer of Karonga, Malawi. Environ Earth Sci 76(9):335

Marchitto TM (2013) Encyclopedia of Quaternary Science (2nd edn). In: Scott A. Elias, Cary J. Mock(eds), Paleoceanography, physical and chemical proxies|Nutrient Proxies, Elsevier, pp 899–906, ISBN 9780444536426. https://doi.org/10.1016/B978-0-444-53643-3.00291-0

Martin JM, Whitfield M (1983) The significance of the river input of chemical elements to the ocean. In: Wong CS, Boyle E, Bruland KW, Burton JD, Goldberg ED (eds) Trace metals in sea water. NATO conference series, vol 9. Springer, Boston, MA

Mathew R, Winterwerp JC (2020) Sediment dynamics and transport regimes in a narrow microtidal estuary. Ocean Dyn 70(4):435–462. https://doi.org/10.1007/s10236-020-01345-9

Matson EA, Brinson MM (1985) Sulfate enrichments in estuarine waters of North Carolina. Estuaries 8(3):279–289

Mayer LM (1982) Aggregation of colloidal iron during estuarine mixing: kinetics, mechanism, and seasonality. Geochim Cosmochim Acta 46(12):2527–2535

Mehta AJ (1989) On estuarine cohesive sediment suspension behavior. J Geophys Res: Oceans 94(C10):14303–14314

Mohamed CARPS, Yaacob WZW (2019) Distribution of chromium and gallium in the total suspended solid and surface sediments of Sungai Kelantan, Kelantan, Malaysia. Sains Malaysiana 48(11):2343–2353

Mook WG, Koene BKS (1975) Chemistry of dissolved inorganic carbon in estuarine and coastal brackish waters. Estuar Coast Mar Sci 3(3):325–336

Mori C, Santos IR, Brumsack HJ, Schnetger B, Dittmar T, Seidel M (2019) Non-conservative behavior of dissolved organic matter and trace metals (Mn, Fe, Ba) driven by porewater exchange in a subtropical mangrove-estuary. Front Mar Sci 6:481

Moses CO, Nordstrom DK, Herman JS, Mills AL (1987) Aqueous pyrite oxidation by dissolved oxygen and by ferric iron. Geochim Cosmochim Acta 51(6):1561–1571

Mucci A, Starr M, Gilbert D, Sundby B (2011) Acidification of lower St. Lawrence Estuary bottom waters. Atmos-Ocean 49(3):206–218

Müller B, Meyer JS, Gächter R (2018) Alkalinity and nitrate concentrations in calcareous watersheds: Are they linked, and is there an upper limit to alkalinity? Biogeosciences Discuss. [preprint]. https://doi.org/10.5194/bg-2018-461

Naciri W, Boom A, Payne MJ, Browne N, Evans NJ, Holdship P, Rankenburg K, Nagarajan R, McDonald BJ, McIlwain J, Zinke J (2023) Massive corals record deforestation in Malaysian Borneo through sediments in river discharge. Biogeosciences 20:1587–1604. https://doi.org/10.5194/bg-2022-235

Naderi M, Raeisi E, Zarei M (2016) The impact of halite dissolution of salt diapirs on surface and ground water under climate change, South-Central Iran. Environ Earth Sci 75(8):708

Nagarajan R, Armstrong-Altrin JS, Kessler FL, Hidalgo-Moral EL, Dodge-Wan D, Taib NI (2015) Provenance and tectonic setting of Miocene siliciclastic sediments, Sibuti Formation, northwestern Borneo. Arab J Geosci 8(10):8549–8565

Nagarajan R, Armstrong-Altrin JS, Kessler FL, Jong J (2017a) Petrological and geochemical constraints on provenance, paleoweathering and tectonic setting of clastic sediments from the Neogene Lambir and Sibuti Formations, NW Borneo. In: Mazumder R (ed) Sediment Provenance: influences on compositional change from source to sink. Elsevier Amsterdam, Netherlands, pp 123–153. https://doi.org/10.1016/B978-0-12-803386-9.00007-1

Nagarajan R, Roy PD, Kessler FL, Jong J, Dayong V, Jonathan MP (2017b) An integrated study of geochemistry and mineralogy of the Upper Tukau Formation, Borneo Island (East Malaysia): sediment provenance, depositional setting and tectonic implications. J Asian Earth Sci 143:77–94

Nagarajan R, Anandkumar A, Hussain SM, Jonathan MP, Ramkumar Mu, Eswaramoorthi S, Saptoro A, Chua HB, (2019) Geochemical characterization of beach sediments of the NW Borneo, SE Asia: implications on provenance, weathering intensity and assessment of coastal environmental status. In: Ramkumar Mu, Arthur James RA, Menier D, Kumaraswamy K (eds) Coastal Zone Management: global Perspectives, Regional Processes, Local Issues, pp 279–330

Nagarajan R, Sharveen R, Abdulmajid A, Jong J, Roy PD, Srinivasalu S (2022) Paragenetic conditions of concretions in the Neogene clastic sediments of NW Borneo: evidence from morphological, petrographic, mineralogical and geochemical data. J Geointerface 1(2):6–20

Namieśnik J, Rabajczyk A (2010) The speciation and physico-chemical forms of metals in surface waters and sediments. Chem Speciat Bioavailab 22(1):1–24

Nieto JM, Sarmiento AM, Olías M, Canovas CR, Riba I, Kalman J, Delvalls TA (2007) Acid mine drainage pollution in the Tinto and Odiel rivers (Iberian Pyrite Belt, SW Spain) and bioavailability of the transported metals to the Huelva Estuary. Environ Int 33(4):445–455

Nystrand MI, Österholm P, Yu C, Åström M (2016) Distribution and speciation of metals, phosphorus, sulfate and organic material in brackish estuary water affected by acid sulfate soils. Appl Geochem 66:264–274

Oldham VE, Miller MT, Jensen LT, Luther GW III (2017) Revisiting Mn and Fe removal in humic rich estuaries. Geochim Cosmochim Acta 209:267–283

Ongetta S, Prasanna MV, Chidambaram S, Nagarajan R, Kuek Clem (2022) Delineation of highland saline groundwater sources in Ba'kelalan region of NE Borneo to improve the salt-making production using geochemical and geophysical approaches. Chemosphere 307(1):135721

Pađan J, Marcinek S, Cindrić AM, Layglon N, Lenoble V, Salaün P ,..., Omanović D (2019) Improved voltammetric methodology for chromium redox speciation in estuarine waters. Analytica Chimica Acta 1089:40–47

Patra S, Liu CQ, Wang FS, Li SL, Wang BL (2012) Behavior of major and minor elements in a temperate river estuary to the coastal sea. Int J Environ Sci Technol 9(4):647–654

Pavoni E, Crosera M, Petranich E, Faganeli J, Klun K. Oliveri P, ..., Adami G (2021) Distribution, mobility and fate of trace elements in an estuarine system under anthropogenic pressure: the case of the Karstic Timavo River (Northern Adriatic Sea, Italy). Estuaries and Coasts 1–17

Peng LC, Leman MS, Hassan K, Nasib BM, Karim R (2004) Stratigraphic Lexicon of Malaysia. Geological Society of Malaysia, Kuala Lumpur, p 162

Perkin E (2013) Titan MPS™ microwave sample preparation system. A reference notebook of microwave applications. Waltham, MA, p 214

Piper AM (1944) A graphic procedure in the geochemical interpretation of water-analyses. EOS Trans Am Geophys Union 25(6):914–928

Pobi KK, Satpati S, Dutta S, Nayek S, Saha RN, Gupta S (2019) Sources evaluation and ecological risk assessment of heavy metals accumulated within a natural stream of Durgapur industrial zone, India, by using multivariate analysis and pollution indices. Appl Water Sci 9(3):58

Prabakaran K, Eswaramoorthi S, Nagarajan R, Anandkumar A, Franco FM (2020) Geochemical behaviour and risk assessment

of trace elements in a tropical river, Northwest Borneo. Chemosphere 252:126430

Prasanna MV, Chidambaram S, Hameed AS, Srinivasamoorthy K (2010) Study of evaluation of groundwater in Gadilam basin using hydrogeochemical and isotope data. Environ Monit Assess 168(1–4):63–90

Priya KL, Jegathambal P, James EJ (2014) Trace metal distribution in a shallow estuary. Toxicol Environ Chem 96(4):579–593

Qin J, Enya O, Lin C (2018) Dynamics of Fe, Mn, and Al liberated from contaminated soil by low-molecular-weight organic acids and their effects on the release of soil-borne trace elements. Appl Sci 8(12):2444

Ralston DK, Warner JC, Geyer WR, Wall GR (2013) Sediment transport due to extreme events: the Hudson River estuary after tropical storms Irene and Lee. Geophys Res Lett 40(20):5451–5455

Ravikumar P, Somashekar RK (2017) Principal component analysis and hydrochemical facies characterization to evaluate groundwater quality in Varahi River basin, Karnataka state, India. Appl Water Sci 7(2):745–755

Regnier P, Wollast R (1993) Distribution of trace metals in suspended matter of the Scheldt estuary. Mar Chem 43(1–4):3–19

Reiman JH, Xu YJ, He S, DelDuco EM (2018) Metals geochemistry and mass export from the Mississippi-Atchafalaya River system to the Northern Gulf of Mexico. Chemosphere 205:559–569

Sabarathinam C, Rashid T, Al-Qallaf H, Hadi K, Bhandary H (2020) Paleoclimatic investigations using isotopic signatures of the Late Pleistocene-Holocene groundwater of the stratified aquifers in Kuwait. J Hydrol 588:125111

Saifullah ASM, Idris MH, Rajaee AH, Johan I (2014) Seasonal variation of water characteristics in Kuala Sibuti River estuary in Miri, Sarawak. Malaysia MJS 33(1):9–22

Salas-Monreal D, Valle-Levinson A (2008) Sea-level slopes and volume fluxes produced by atmospheric forcing in estuaries: Chesapeake Bay case study. J Coastal Res 24:208–217

Sassi MG, Hoitink AJF (2013) River flow controls on tides and tides-mean water level profiles in a tidal freshwater river. J Geophys Res: Oceans 118(9):4139–4151

Schoeller H (1967) Qualitative evaluation of ground water resources (in methods and techniques of groundwater investigations and development), water Resources Series. UNESCO 33:44–52

Scott CR, Hemingway KL, Elliot M, de Jonge VN, Pethick JS, Malcolm S, Wilkinson M (1999) Impacts of nutrients in estuaries: phase 2, summary report. R&D Technical Report P269. Environ Agency Bristol 28

Sedeño-Díaz JE, López-López E, Mendoza-Martínez E, Rodríguez-Romero AJ, Morales-García SS (2020) Distribution coefficient and metal pollution index in water and sediments: proposal of a new index for ecological risk assessment of metals. Water 12(1):29

Senthilkumar S, Balasubramanian N, Gowtham B, Lawrence JF (2017) Geochemical signatures of groundwater in the coastal aquifers of Thiruvallur district, south India. Appl Water Sci 7(1):263–274

Shapiro J (1964) Effect of yellow organic acids on iron and other metals in water. J Am Water Works Ass 56(8):1062–1082

Sholkovitz ER (1976) Flocculation of dissolved organic and inorganic matter during the mixing of river water and seawater. Geochim Cosmochim Acta 40(7):831–845

Sholkovitz E, Szymczak R (2000) The estuarine chemistry of rare earth elements: comparison of the Amazon, Fly, Sepik and the Gulf of Papua systems. Earth Planet Sci Lett 179(2):299–309

Sia SG, Abdullah WH (2012) Enrichment of arsenic, lead, and antimony in Balingian coal from Sarawak, Malaysia: modes of occurrence, origin, and partitioning behaviour during coal combustion. Int J Coal Geol 101:1–15

Simon K, Hassan MHA, Barbeito MPJ (2014) Sedimentology and stratigraphy of the Miocene Kampung Opak limestone (Sibuti Formation), Bekenu, Sarawak. Bull Geol Soc Malaysia 60:45–53

Sivasubramanian P, Balasubramanian N, Soundranayagam JP, Chandrasekar N (2013) Hydrochemical characteristics of coastal aquifers of Kadaladi, Ramanathapuram District, Tamilnadu, India. Appl Water Sci 3(3):603–612

Söderlund M, Virkanen J, Holgersson S, Lehto J (2016) Sorption and speciation of selenium in boreal forest soil. J Environ Radioact 164:220–231

Somura H, Takeda I, Arnold JG, Mori Y, Jeong J, Kannan N, Hoffman D (2012) Impact of suspended sediment and nutrient loading from land uses against water quality in the Hii River basin, Japan. J Hydrol 450:25–35

Srinivasamoorthy K, Gopinath M, Chidambaram S, Vasanthavigar M, Sarma VS (2014) Hydrochemical characterization and quality appraisal of groundwater from Pungar sub basin, Tamilnadu, India. J King Saud Univ-Sci 26(1):37–52

Tchounwou PB, Yedjou CG, Patlolla AK, Sutton DJ (2012) Heavy metal toxicity and the environment. Mol Clin Environ Toxicol 101:133–164

Tenaga KTA (2003) Updating of condition of flooding in Malaysia–main report. Drainage and Irrigation Department, Kuala Lumpur. Retrieved from https://www.water.gov.my/jps/resources/auto%20download%20images/5844e46d37d56.pdf.

Tessier APGC, Campbell PGC, Auclair JC, Bisson M (1984) Relationships between the partitioning of trace metals in sediments and their accumulation in the tissues of the freshwater mollusc Elliptio complanata in a mining area. Can J Fish Aquat Sci 41(10):1463–1472

Thivya C, Chidambaram S, Thilagavathi R, Prasanna MV, Singaraja C, Adithya VS, Nepolian M (2015) A multivariate statistical approach to identify the spatio-temporal variation of geochemical process in a hard rock aquifer. Environ Monit Assess 187(9):552

Thivya C, Chidambaram S, Rao MS, Gopalakrishnan M, Thilagavathi R, Prasanna MV, Nepolian M (2016) Identification of recharge processes in groundwater in hard rock aquifers of Madurai District using stable isotopes. Environmental Processes 3(2):463–477

Tian R (2020) Factors controlling hypoxia occurrence in estuaries, Chester River, Chesapeake Bay. Water 12(7):1961

Tomczak W, Boyer P, Krimissa M, Radakovitch O (2019) Kd distributions in freshwater systems as a function of material type, mass-volume ratio, dissolved organic carbon and pH. Appl Geochem 105:68–77

Tosca NJ, Jiang CZ, Rasmussen B, Muhling J (2019) Products of the iron cycle on the early Earth. Free Radic Biol Med 140:138–153

Turner A (1996) Trace-metal partitioning in estuaries: importance of salinity and particle concentration. Mar Chem 54(1–2):27–39

Turner A, Millward GE (2000) Particle dynamics and trace metal reactivity in estuarine plumes. Estuar Coast Shelf Sci 50(6):761–774

Uncles RJ, Elliott RCA, Weston SA (1985) Observed fluxes of water, salt and suspended sediment in a partly mixed estuary. Estuar Coast Shelf Sci 20(2):147–167

USEPA (1992) (Digitally published: 2017, January 27). SW-846 test method 3005A: acid digestion of waters for total recoverable or dissolved metals for analysis by flame atomic absorption (FLAA) or inductively coupled plasma (ICP) spectroscopy. Retrieved from https://www.epa.gov/hw-sw846/sw-846-test-method-3005a-acid-digestion-waters-total-recoverable-or-dissolved-metals

Valappil NKM, Viswanathan PM, Hamza V, Sabarathinam C (2022) Isoscapes to address the regional precipitation trends in the equatorial region of Southeast Asia. Physics and Chemistry of the Earth, Parts A/B/C 127:103159

Van Dam BR, Wang H (2019) Decadal-scale acidification trends in adjacent North Carolina estuaries: competing role of anthropogenic CO2 and riverine alkalinity loads. Front Mar Sci 6:136

Vinh VD, Ouillon S (2021) The double structure of the Estuarine Turbidity Maximum in the Cam-Nam Trieu mesotidal tropical estuary. Vietnam Marine Geology 442:106670

Walker LM, Montagna PA, Hu X, Wetz MS (2021) Timescales and magnitude of water quality change in three Texas estuaries induced by passage of Hurricane Harvey. Estuar Coasts 44:960–971

Wei X, Garnier J, Thieu V, Passy P, Le Gendre R, Billen G, Akopian M, Laruelle GG (2022) Nutrient transport and transformation in macrotidal estuaries of the French Atlantic coast: a modeling approach using the carbon-generic estuarine model. Biogeosciences 19:931–955. https://doi.org/10.5194/bg-19-931-2022

Wen Y, Xiao J, Goodman BA, He X (2019) Effects of organic amendments on the transformation of Fe (oxyhydr) oxides and soil organic carbon storage. Front Earth Sci 7:257

Weng CH, Huang CP, Allen HE, Cheng AD, Sanders PF (1994) Chromium leaching behavior in soil derived from chromite ore processing waste. Sci Total Environ 154(1):71–86

Weng CH, Huang CP, Sanders PF (2001) Effect of pH on Cr (VI) leaching from soil enriched in chromite ore processing residue. Environ Geochem Health 23(3):207–211

Wollast R, Billen G, Duinker JC (1979) Behaviour of manganese in the Rhine and Scheldt estuaries: I. Physico-chemical aspects. Estuarine Coastal Mar Sci 9(2):161–169

Yang X, Wang ZL (2017) Distribution of dissolved, suspended, and sedimentary heavy metals along a salinized river continuum. J Coastal Res 33(5):1189–1195

Yudovich YE, Ketris MP (2006) Selenium in coal: a review. Int J Coal Geol 67(1–2):112–126

Zaharah AR, Gikonyo EW, Silek B, Goh KJ, Amin S (2014) Evaluation of phosphate rock sources and rate of application on oil palm yield grown on peat soils of Sarawak, Malaysia. J Agron 13(1):12–22

Zhang JZ, Huang XL (2011) Effect of temperature and salinity on phosphate sorption on marine sediments. Environ Sci Technol 45(16):6831–6837

Zhang J, Zhou F, Chen C, Sun X, Shi Y, Zhao H, Chen F (2018) Spatial distribution and correlation characteristics of heavy metals in the seawater, suspended particulate matter and sediments in Zhanjiang Bay. China Plos One 13(8):e0201414

Zhang C, Yu ZG, Zeng GM, Jiang M, Yang ZZ, Cui F, ..., Hu L (2014) Effects of sediment geochemical properties on heavy metal bioavailability. Environ Int 73:270–281

Zhang X, Müller M, Jiang S, Wu Y, Zhu X, Mujahid A, ..., Zhang J (2020) Distribution and flux of dissolved iron in the peatland-draining rivers and estuaries of Sarawak, Malaysian Borneo. Biogeosciences 17(7):1805–1819

Zheng S, Wang P, Wang C, Hou J, Qian J (2013) Distribution of metals in water and suspended particulate matter during the resuspension processes in Taihu Lake sediment, China. Quatern Int 286:94–102

Zhou JL, Liu YP, Abrahams PW (2003) Trace metal behaviour in the Conwy estuary, North Wales. Chemosphere 51(5):429–440

Zhou Q, Liu Y, Li T, Zhao H, Alessi DS, Liu W, Konhauser KO (2020) Cadmium adsorption to clay-microbe aggregates: implications for marine heavy metals cycling. Geochim Cosmochim Acta 290:124–136

Zhu W, Wang C, Hill J, He Y, Tao B, Mao Z, Wu W (2018) A missing link in the estuarine nitrogen cycle? Coupled nitrification-denitrification mediated by suspended particulate matter. Sci Rep 8(1):1–10